OPEN

Smooth Muscle Enriched Long Noncoding RNA (*SMILR*) Regulates Cell Proliferation

Margaret D. Ballantyne, MRes; Karine Pinel, PhD; Rachel Dakin, PhD; Alex T. Vesey, MD; Louise Diver, PhD; Ruth Mackenzie, PhD; Raquel Garcia, PhD; Paul Welsh, PhD; Naveed Sattar, MD, PhD; Graham Hamilton, PhD; Nikhil Joshi, MD, PhD; Marc R. Dweck, MD, PhD; Joseph M. Miano, PhD; Martin W. McBride, PhD; David E. Newby, MD, PhD; Robert A. McDonald, PhD; Andrew H. Baker, PhD

Background—Phenotypic switching of vascular smooth muscle cells from a contractile to a synthetic state is implicated in diverse vascular pathologies, including atherogenesis, plaque stabilization, and neointimal hyperplasia. However, very little is known about the role of long noncoding RNA (lncRNA) during this process. Here, we investigated a role for lncRNAs in vascular smooth muscle cell biology and pathology.

Methods and Results—Using RNA sequencing, we identified >300 lncRNAs whose expression was altered in human saphenous vein vascular smooth muscle cells following stimulation with interleukin-1α and platelet-derived growth factor. We focused on a novel lncRNA (Ensembl: RP11-94A24.1), which we termed smooth muscle–induced lncRNA enhances replication (*SMILR*). Following stimulation, *SMILR* expression was increased in both the nucleus and cytoplasm, and was detected in conditioned media. Furthermore, knockdown of *SMILR* markedly reduced cell proliferation. Mechanistically, we noted that expression of genes proximal to *SMILR* was also altered by interleukin-1α/platelet-derived growth factor treatment, and *HAS2* expression was reduced by *SMILR* knockdown. In human samples, we observed increased expression of *SMILR* in unstable atherosclerotic plaques and detected increased levels in plasma from patients with high plasma C-reactive protein.

Conclusions—These results identify *SMILR* as a driver of vascular smooth muscle cell proliferation and suggest that modulation of *SMILR* may be a novel therapeutic strategy to reduce vascular pathologies. **(*Circulation*. 2016;133:2050-2065. DOI: 10.1161/CIRCULATIONAHA.115.021019.)**

Key Words: atherosclerosis ■ cell proliferation ■ microRNAs ■ RNA, untranslated ■ plasma protein, human

Vessel wall remodeling is an integral pathological process central to cardiovascular diseases including atherogenesis, plaque rupture, and neointimal hyperplasia–associated vein graft failure and in-stent restenosis.[1,2] Resident vascular smooth muscle cells (VSMCs) are typically quiescent and contractile in the normal physiological state. However, following pathological or iatrogenic vascular injury, the release of cytokines and growth factors from VSMCs, aggregated platelets, and inflammatory cells on the damaged intimal surface leads to phenotypic switching of VSMCs and the adoption of a more synthetic, pro-proliferative, and promigratory state.[3] In the setting of the pathological injury of atherosclerosis, VSMCs not only contribute to the atherogenic process itself but can also engender plaque stabilization through the generation of a thick-capped fibroatheroma. For acute iatrogenic vascular injury, overexuberant proliferation of VSMC subpopulations promotes neointimal hyperplasia leading to luminal narrowing such as seen in vein graft failure or in-stent restenosis.[4] Phenotypic switching of VSMCs and release of cytokines and growth factors are therefore critical in vascular disease, and understanding the mechanisms involved is critical to gain insights into the pathology and identify new opportunities for therapies.

Clinical Perspective on p 2065

The highly conserved interleukin-1α (IL1α) and platelet-derived growth factor (PDGF) pathways play prominent roles in VSMC-associated pathologies.[1,5] IL1α is a central mediator in the cytokine cascade and a potent activator of vascular cytokine production. Furthermore, previous studies have

Received July 28, 2015; accepted March 28, 2016.

From BHF Glasgow Cardiovascular Research Centre, University of Glasgow, United Kingdom (M.D.B., R.D., L.D., R.M., R.G., P.W., N.S., M.W.N., R.A.M., A.H.B.); British Heart Foundation/University of Edinburgh Centre for Cardiovascular Science, Edinburgh, United Kingdom (M.D.B., K.P., A.T.V., N.J., M.R.D., D.E.N., R.A.M., A.H.B.); Glasgow Polyomics, College of Medical, Veterinary and Life Sciences, The University of Glasgow, United Kingdom (G.H.); and Aab Cardiovascular Research Institute, University of Rochester School of Medicine and Dentistry, NY (J.M.M.).

The online-only Data Supplement is available with this article at http://circ.ahajournals.org/lookup/suppl/doi:10.1161/CIRCULATIONAHA.115.021019/-/DC1.

Correspondence to Andrew H. Baker, PhD, BHF Glasgow Cardiovascular Research Centre, 126 University Place, University of Glasgow, Glasgow G12 8TA, United Kingdom. E-mail andrew.h.baker@glasgow.ac.uk

demonstrated that ligation injury results in reduced neointimal formation in IL1 receptor knockout mice.[6] Downstream mediators include the signaling molecules MEKK1 and p38 and the transcription factor NF-κB that activate mediators of inflammation and cellular migration.[7] PDGF is a potent mitogen and chemoattractant, and expression is increased following vascular injury.[8] Conversely, a reduction in PDGF expression reduces intimal thickening and cellular content of the neointima.[9] Activation of both IL1α and PDGF signaling pathways simultaneously can activate common downstream targets leading to additive or synergistic effects. This includes activation of NF-κB leading to the upregulation of metalloproteinase 3 and 9,[10] genes critical in the development of vasculoproliferative pathologies.

Over the past decade, there has been substantial interest in determining the complex interactions between hierarchical levels of gene regulation. Up to 90% of the human genome is transcribed at different developmental stages and only ≈2% of RNA molecules are translated into protein.[11] The functional complexity of organisms therefore appears to be reliant on noncoding RNA molecules. Noncoding RNAs are subdivided into several classes, including microRNA (miRNA) and long noncoding RNA (lncRNA). miRNAs are abundantly expressed in vascular tissues and play an important role in vascular pathology. Interestingly, recent studies have demonstrated that miRNAs are capable of being released into the blood from injured cells. These miRNAs are relatively stable and have been reported as biomarkers for several disease states, including myocardial infarction[12] and heart failure.[13,14] Although the role of miRNAs is reasonably established in the setting of cardiovascular pathology, relatively little is known about the role of lncRNAs. lncRNAs are capable of regulating target DNA, RNA, and protein at the pre- and posttranscriptional level. It is becoming clear that lncRNAs play a pivotal role in cellular physiology and pathology via localization in subpopulations of cells and through highly controlled temporal expression.[15] However, detailed insights into their regulation and biological roles are only beginning to emerge. In the vascular setting, *SENCR* and *MALAT1* have been implicated in the control of vascular cell migration and endothelial cell sprouting, respectively.[16,17] Interestingly, *SENCR* is implicated in phenotypic switching of VSMCs to a more promigratory phenotype because knockdown of this lncRNA downregulates contractile genes.[17] A greater understanding of lncRNAs in quiescent and proliferative VSMCs may provide valuable insight into the specific roles of lncRNAs in response to pathological processes.

Methods

Human Tissue Samples

Surplus human saphenous vein tissue was obtained from patients undergoing coronary artery bypass grafting. Carotid plaques were obtained from patients undergoing endarterectomy following an acute and symptomatic neurovascular event. Human plasma samples were used from a previously published study: Carotid Ultrasound and Risk of Vascular disease in Europeans and South Asians (CURVES).[2] All patients gave their written, informed consent. All procedures had local ethical approval (06/S0703/110, 12/WS/0227, 09/S0703/118, and 12/NW/0036). All studies were approved by East and West Scotland Research Ethics Committees, and all experiments were conducted according to the principles expressed in the Declaration of Helsinki.

Tissue and Cell Culture

All cells were maintained at 37°C in a humidified atmosphere containing 5% CO_2. Primary human saphenous vein–derived endothelial cells (HSVECs) were isolated by a modified version of the protocol described by Jaffe and colleagues[18] and maintained in large-vessel endothelial cell culture medium supplemented with 20% fetal calf serum (Life Technologies, Paisley, UK). Primary human saphenous vein–derived smooth muscle cells (HSVSMCs) were isolated from medial explants[19] and maintained in Smooth Muscle Cell Growth Medium 2 (PromoCell, Heidelberg, Germany) with supplements. Human coronary artery VSMCs were purchased from Lonza (Basel, Switzerland) and maintained in VSMC media as above.

Sample Preparation for RNA-seq Library Construction and Analysis

HSVSMCs were plated, quiesced in medium containing 0.2% fetal calf serum for 48 hours before the stimulation with 10 ng/mL IL1α, 20 ng/mL PDGF (R&D Systems) or a combination of both for 72 hours. Total RNA was processed through miRNeasy kit (Qiagen, Hilden, Germany) following the manufacturer's instructions, treated with DNase 1 (amplification grade; Sigma, St. Louis, MO) to eliminate genomic DNA contamination and quantified by using a NanoDrop ND-1000 Spectrophotometer (Nano-Drop Technologies, Wilmington, DE). Following bioanalyzer quality control for RNA integrity number values >8, RNA sequencing (RNA-seq) was performed on ribosomal-depleted RNA using an Illumina Hiseq platform by Beckman Coulter Genomics. Paired-end sequencing was performed with a read depth of 70 million (n=4/group). RNA-seq reads were processed and trimmed to ensure quality, adapter sequences were removed using Flexbar[20] and mapped to the Ensembl annotation of GRCh37.75 using the TopHat2 version 2.0.9.[21] The transcriptome was assembled from the aligned reads and quantified using Cufflinks version 2.2.1.[22] The differential expression levels between the groups were assessed using Cuffdiff version 2.2.1.[23] The data set is deposited in the Gene Expression Omnibus (GEO) repository, study number GSE69637. The biotype of each transcript was annotated according to the Ensembl database. Normalization and statistical analysis of differentially expressed transcripts were performed by using edgeR and data filtered to find transcripts that were differentially expressed (P<0.01) between 0.2% media and each treatment group. Differentially expressed lncRNAs, between control and both IL1α/PDGF treatments, were explored by using more stringent criteria (P<0.01, false discover rate [FDR] <0.01, log fold change>2) and filtered according to transcript abundance (fragments per kilobase of exon per million fragments mapped [FPKM]>1 in at least 1 group). Data outputs such as pie charts and heatmaps were generated using R. Ingenuity pathway analysis was performed by using protein-coding genes differentially expressed (FDR<0.01) from Edge R analysis.

Assessment of RNA Secretion From HSVSMC

RNA extraction on conditioned HSVSMC media was performed by using a standard volume (2 mL). The conditioned media was first centrifuged (10 minutes; 2000*g*; 4°C) to remove all cells and debris. After addition of 1.4 mL of QIAzol (Qiagen), 3 μL of *Caenorhabditis elegans* total RNA at 25 ng/μL was added to each sample. Following 5-minute incubation at room temperature, 140 μL of chloroform was added and samples centrifuged (15 minutes; 15 000*g*; 4°C). The clear upper aqueous phase was used to isolate RNA by using the miRNEasy mini kit (Qiagen) as previously described with alteration of the final wash step (75% ethanol in diethylpyrocarbonate water). Different quantities of total RNA were spiked and a dose-response effect was observed (Figure IA in the online-only Data Supplement). The quality of the amplicon was assessed via analysis of melting curves (Figure IB in the online-only Data Supplement) and subsequent visualization on agarose gel (Figure IC in the online-only Data Supplement). This showed a unique amplification product corresponding to the cDNA fragment of *ama-1*. Because of the correlation observed between the quantity of spike-in and *ama-1* expression (Figure ID in the online-only

Data Supplement), we used 75 ng in all subsequent extractions. This amount allowed reproducibility of our method, with the Ct values of *ama-1* being 29.4±0.3 across 5 separate extractions in nonconditioned media (Figure IE in the online-only Data Supplement).

Gene Expression qRT-PCR

For gene expression analysis, cDNA for mRNA analysis was obtained from total RNA using the Multiscribe Reverse Transcriptase (Life Technologies, Paisley, UK). Quantitative real-time polymerase chain reaction (qRT-PCR) was performed using Power SYBR green (Life Technologies) with custom PCR primers (Eurofins MWG, Ebersberg, Germany), the specificity of these primers was confirmed by performing a melting curve and running their PCR produce on a gel (Table I in the online-only Data Supplement – primer sequences). Ubiquitin C was selected as housekeeping gene because of its stability across all groups studied. Fold changes were calculated by using the $2^{-\Delta\Delta^{Ct}}$ method.[23]

Statistical Analysis

Statistical analysis was performed according to figure legends. Data in graphs are shown on relative expression scales as referenced by Livak and Schmittgen.[24] Data are given as both mean±standard deviation (shown as bars and whiskers) and also as the individual points to clearly represent the data. Note that as the relative expression scale is inherently skewed; the bars indicate the geometric mean of the relative expression fold change, and the standard deviation whiskers denote the relative expression fold change equivalent to an increase of 1 standard deviation above the mean on the log-transformed scale. All statistical analysis is performed on the dCt scale (a logarithmic transformation of the data shown on the relative quantification in the plots).[24] No evidence of unequal variances across groups was found for any of analyses of the dCt scale data using the Levene test on Minitab version 17 before statistical analysis. Comparisons between 2 groups were analyzed using 2-tailed unpaired or paired Student *t* test. One-way analysis of variance with Tukey post hoc or 1-way analysis of variance multiple-comparisons test for pooled samples, via Graph Pad Prism version 5.0, was used for comparisons among ≥3 groups. Statistical significance is denoted by a *P* value of <0.05.

Results

Induction of Inflammatory and Cell Cycle Pathways by IL1α and PDGF

We sought to identify lncRNAs that are regulated during the induction of proliferative and inflammatory pathways in HSVSMCs. RNAs were identified by using RNA-seq of HSVSMC treated for 72 hours (Figure 1A). Activation of the IL1α and PDGF signaling pathways was confirmed by the presence of the inflammatory miRNA miR-146a (Figure1B) and induction of VSMC proliferation (Figure 1C). The RNA sequencing obtained an average of 70 million reads per sample, with 93.5% aligning to the GRCh37 genome reference files. The majority of reads, under all conditions, corresponded to mRNA (49.6±0.48%; Figure 1D and Figure IIA in the online-only Data Supplement). To identify the biological function, networks, and canonical pathways that were affected by VSMC stimulation, we performed ingenuity pathway analysis after RNA-seq analysis. Ingenuity pathway analysis confirmed that the mRNAs with altered expression following IL1α treatment were significantly enriched in pathways related to cellular movement and inflammatory disease (Table II in the online-only Data Supplement), whereas PDGF stimulation led to the marked enrichment in cell cycle pathways (Table III in the online-only Data Supplement). Interestingly, costimulation led to enrichment in cell cycle and cardiovascular development pathways (Table IV in the online-only Data Supplement). Further analysis of differentially expressed mRNAs with a stringent cutoff of FDR<0.01 identified 518 protein-coding genes altered following IL1α treatment and 540 following PDGF treatment. Notably, dual stimulation altered 1133 known protein-coding genes with 480 uniquely associated with dual stimulation and not affected by IL1α or PDGF treatment alone (Figure 1E and Figure IIB in the online-only Data Supplement).

Identification of Differentially Expressed lncRNAs in HSVSMCs Treated With IL1α and PDGF

We next assessed whether lncRNAs were dynamically regulated by growth factor and cytokine stimulation. Approximately 33% of reads in each condition aligned to known or predicted lncRNAs (Figure IIIA in the online-only Data Supplement). Differential expression analysis confirmed substantial differences in lncRNA expression between control and stimulated cells. Using the stringent criteria FDR ≤0.01 and log2 fold change ≥2, to declare significance and FPKM >1, to confirm quantifiable expression we identified 224, 215, and 369 differentially expressed lncRNAs following IL1α, PDGF, or dual stimulation, respectively (Figure IIIA in the online-only Data Supplement). Because lncRNAs can typically contain multiple splice variants, the numbers quoted refer to a single consensus gene model and therefore do not reflect the multiple transcripts of each lncRNA. To determine whether specific biotypes of lncRNA were enriched following HSVSMC stimulation, those differentially expressed were further subdivided according to biotype in the Ensembl database. LncRNA biotypes are based on their relative orientation to protein-coding genes; intervening lncRNA (lincRNA), antisense, overlapping and processed transcripts. With the use of control and dual stimulation as an example, the distribution of different lncRNA biotypes was as follows: intervening (45.5%), antisense (45.3%), overlapping (1.4%), and processed transcripts (7.9%; Figure IIIB in the online-only Data Supplement). Focusing on lincRNA, the candidates (control versus IL1α and PDGF, FDR<0.01, log fold change <2, FPKM>1) were ranked according to their FPKM and level of upregulation/downregulation (Figure 2A, Figure IV in the online-only Data Supplement for heat map of all conditions). A subset of the most differentially expressed transcripts was identified and validated by qRT-PCR (RP11-91k9.1, RP11-94a24.1, RP11-709B3.2, RP11-760H22.2, and AC018647.3; Figure 2B, chromosomal locations in Table I in the online-only Data Supplement). This was consistent with the RNA-seq results, showing RP11-94a24.1 and RP11-91k9.1 upregulated 20.2±30– and 45±26.4–fold, respectively, following costimulation and lncRNAs RP11-709B3.2, RP11-760H22.2, and AC018647.3 being downregulated 16-, 28-, and 1209-fold, respectively (Figure 3A; relative quantification=0.06±0.04, 0.035±0.01, and 0.0008±0.001, respectively). The dissociation curves and gel products of each primer set are shown in Figure V in the online-only Data Supplement.

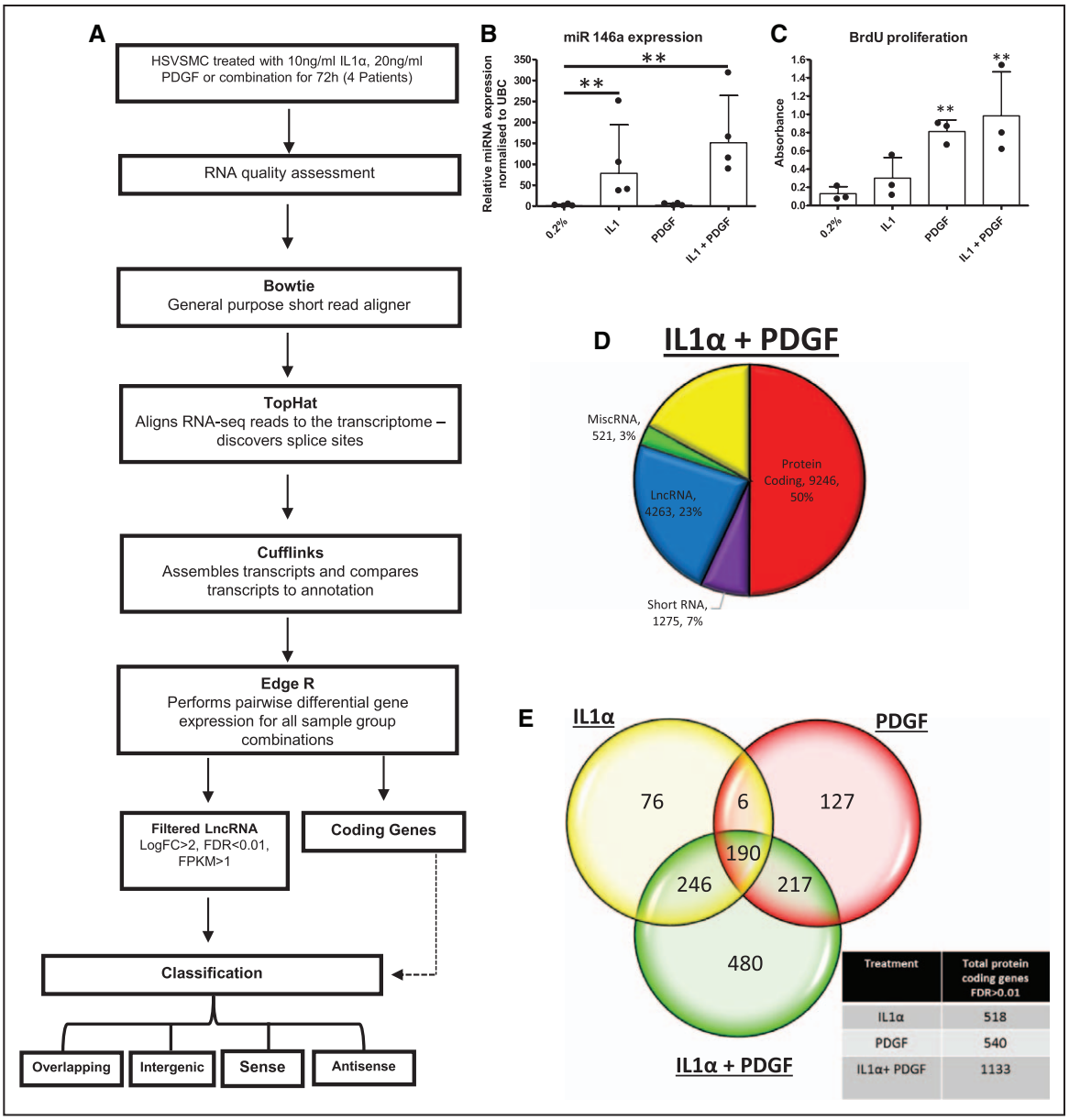

Figure 1. RNA sequencing shows IL1α and PDGF induction of inflammatory and cell cycle pathways. **A**, Study design for determination of the transcriptome in quiescent and stimulated HSVSMCs. HSVSMCs were treated for 72 hours, RNA quality was assessed and subjected to RNA-seq following the Tuxedo pipeline for analysis. **B**, Known inflammatory microRNA, miR146a, is upregulated by IL1α (n=4). ***P*<0.01 vs 0.2% condition. Multiple comparison 1-way ANOVA. **C**, BrdU incorporation as an indirect marker of proliferation was assessed in all patients (n=3). ***P*<0.01 vs 0.2% condition. **D**, Biotype distribution of all transcripts identified by RNA-seq analysis generated from HSVSMCs treated with IL1α and PDGF, cutoff at FPKM>0.1 **E**, Venn diagram indicating overlap of protein-coding genes with altered expression (analyzed using EdgeR, FDR<0.01) across each treatment. ANOVA indicates analysis of variance; BrdU, bromodeoxyuridine; FC, fold change; FDR, false discovery rate; FPKM, fragments per kilobase of exon per million fragments mapped; HSVSMC, human saphenous vein–derived smooth muscle cell; IL1α, interleukin-1α; lncRNA, long noncoding RNA; miR, microRNA; miscRNA, miscellaneous RNA; miRNA, microRNA; PDGF, platelet-derived growth factor; and UBC, ubiquitin C.

Vascular Enriched Expression of RP11-94a24.1

The expression of each lncRNA was quantified in a range of 10 normal human tissues including specimens derived from brain, gastrointestinal, reproductive, and endocrine systems. In general, lncRNAs were expressed at relatively low levels across the tissue panel. However, we observed that RP11-94a24.1 was expressed highest in the heart, whereas RP11-91K9.1 and AC018647.3 showed preferential expression within the liver and brain, respectively. RP11-709B3.2 and RP11-760H22.2 displayed highest expression in the spleen and thyroid, respectively (Figure VIA in the online-only Data Supplement). We next examined the expression of each lncRNA in primary HSVECs, HSVSMCs, and human coronary artery SMCs. All lncRNAs had higher expression in VSMCs of either venous or arterial lineage than in endothelial cells, suggesting VSMC enrichment (Figure VIB in the online-only Data Supplement). We also assessed whether the expression of these lncRNAs could be modulated by IL1α and PDGF in HSVECs as had been found in the HSVSMCs. Notably, subsequent downregulation of

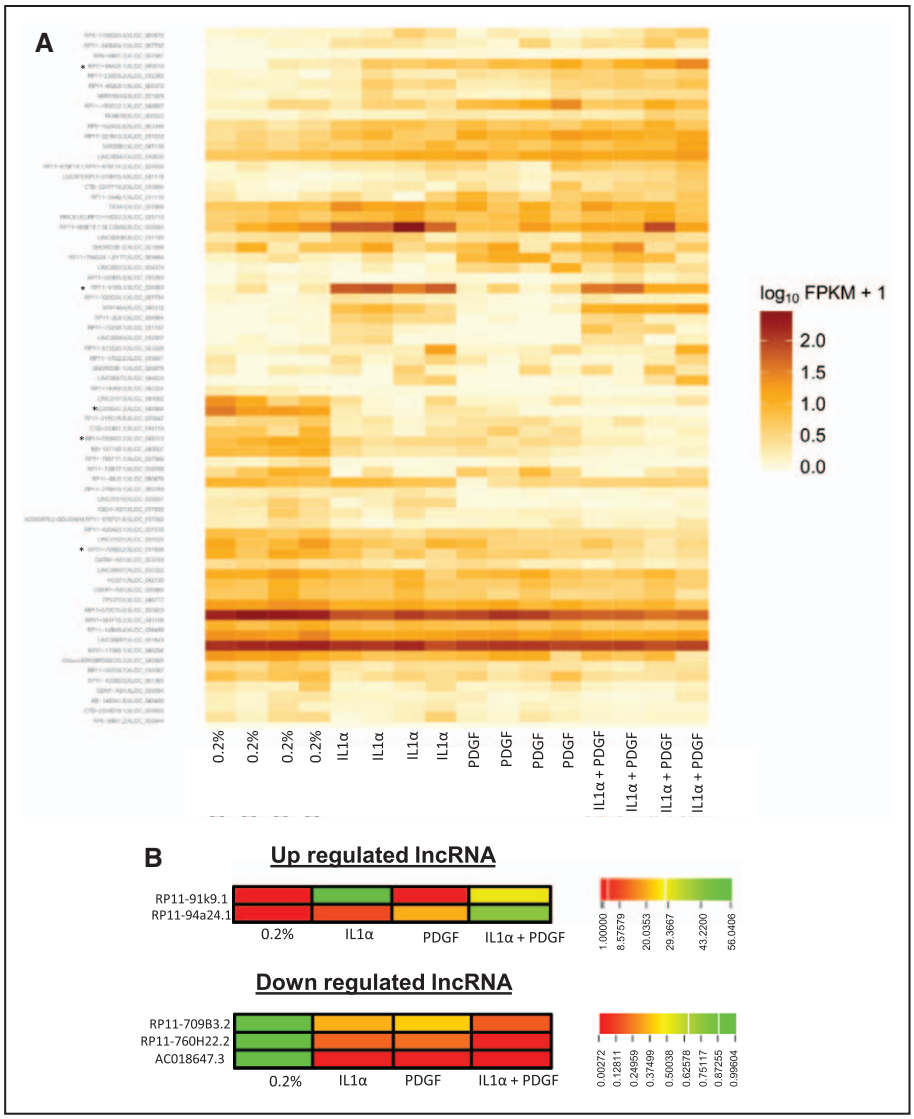

Figure 2. Identification of differentially expressed lncRNAs in HSVSMCs treated with IL1α and PDGF. **A**, Heatmaps showing order of differentially expressed transcripts within the 4 patient samples before and after IL1α/PDGF treatment. lncRNA selected for validation marked by *. **B**, Heatmap representing the fold change of the 5 lncRNAs selected for validation. Heatmaps represent data from RNA-seq pipeline. HSVSMC indicates human saphenous vein–derived smooth muscle cell; IL1α, interleukin-1α; lncRNA, long noncoding RNA; and PDGF, platelet-derived growth factor.

RP11-709B3.2, RP11-760H22.2, and AC018647.3 was not observed in HSVECs as was the case in HSVSMCs (data not shown). Stimulation of HSVECs produced a significant 3.8±0.7– and 8.7±2.1–fold upregulation of RP11-91K9.1 following IL1α and IL1α/PDGF treatment, respectively (Figure 3B). However, stimulation had no effect on RP11-94a24.1 expression (Figure 3B), indicating selective regulation in HSVSMCs. Because of the expression of RP11-94a24.1 in HSVSMCs and its cell-specific induction in response to pathological mediators of vascular injury, we focused further studies on RP11-94a24.1. We termed this lncRNA, *smooth muscle–induced lncRNA enhances replication* (*SMILR*). *SMILR* expression was assessed through the use of 3 independent primer sets targeting differential exons of the lncRNA. qRT-PCR revealed similar Ct and fold changes among the 3 sets, further confirming our previous data (Figure VII in the online-only Data Supplement). The longest open reading frame within *SMILR* is 57 amino acids. Analysis of this open reading frame using the Coding Potential Calculator (http://cpc.cbi.pku.edu.cn) did not reveal any similarity to known protein-coding sequences suggesting that this RNA has no protein-coding potential (data not shown).

IL1α/PDGF Treatment Induces the Expression of *SMILR* in a Time-Dependent Manner

To investigate the longitudinal regulation of *SMILR*, we stimulated HSVSMCs with PDGF, IL1α, or a combination of both (1.5, 4, 24, 48, and 72 hours). We found significant upregulation of *SMILR* in response to PDGF as early as 4 hours after stimulation. By 24 hours, *SMILR* expression was increased by treatment with PDGF or IL1α, and both together, as well (Figure VIII in the online-only Data Supplement). The combination of PDGF and IL1α induced a synergistic increase in *SMILR* expression at 72 hours.

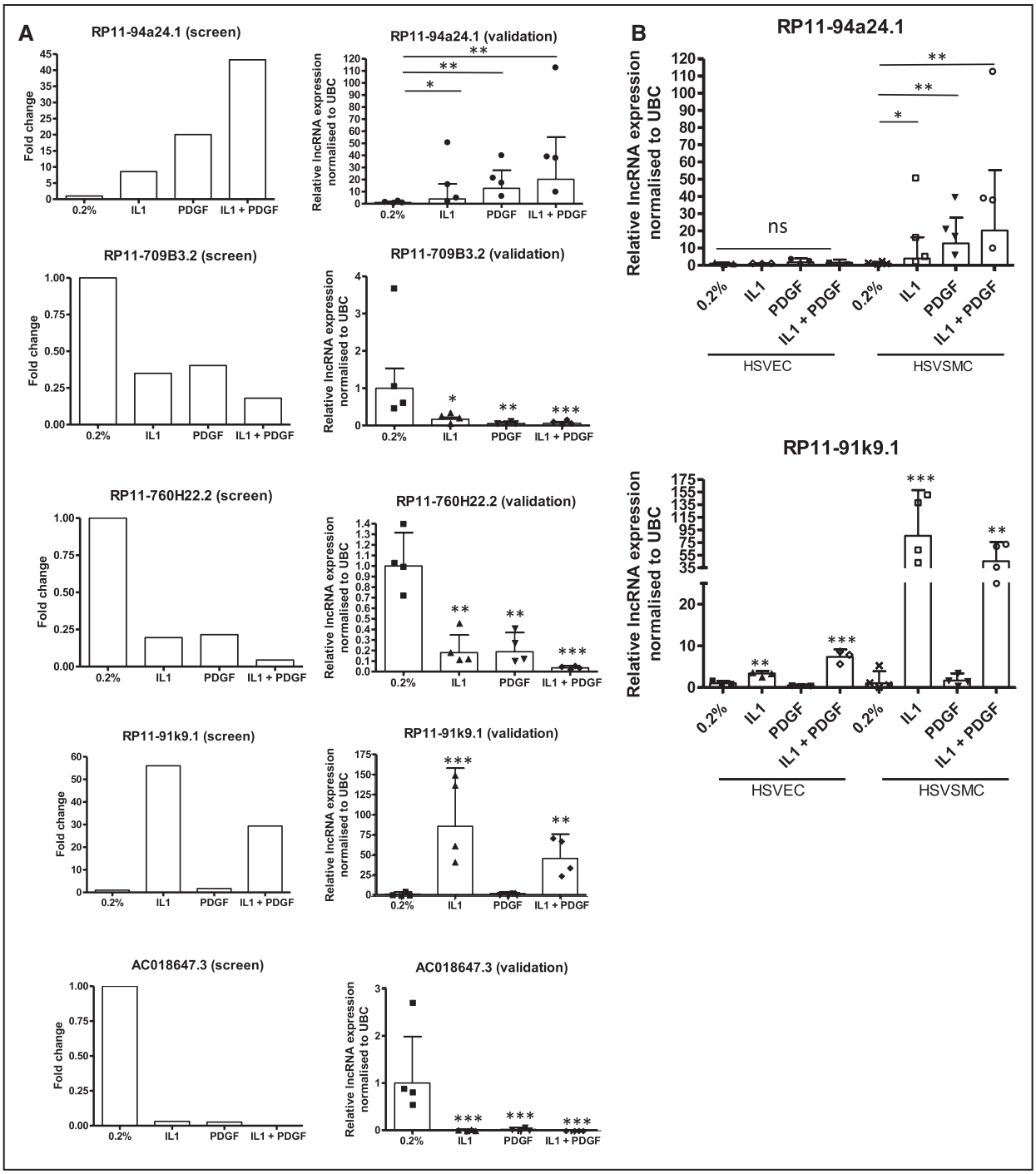

Figure 3. Treatment with IL1α and PDGF significantly altered lncRNA expression and showed distinct expression within vascular cell types. **A**, Graphs indicate fold change of lncRNA from RNA-seq data and subsequent validation by qRT-PCR (n=4). **P*<0.05, ***P*<0.01, ****P*<0.001 vs 0.2% condition. **B**, Basal and stimulated expression of lncRNAs 2 and 7 within HSVEC and HSVSMC (n=4 for SMC and n=3 for EC; **P*<0.05, ***P*<0.01, ****P*<0.001 vs 0.2% in each specific cell type). EC indicates endothelial cell; HSVEC, human saphenous vein–derived endothelial cell; HSVSMC, human saphenous vein–derived smooth muscle cell; IL1α, interleukin-1α; lncRNA, long noncoding RNA; PDGF, platelet-derived growth factor; qRT-PCR, quantitative real-time polymerase chain reaction; SMC, smooth muscle cell; and UBC, ubiquitin U.

Cellular Localization of *SMILR* in HSVSM Cells

Rapid amplification of cDNA ends[25] was used to design specific RNA fluorescent in situ hybridization (FISH) probes. RNA FISH highlighted a *SMILR* isoform, consisting of an additional 6 bp at the 5′ end and 316 bp at the 3′ end (Figure IXA and IXB in the online-only Data Supplement). Rapid amplification of cDNA ends data are supported by the raw RNA-seq files (Figure XA through XC in the online-only Data Supplement).

We performed RNA FISH to provide visuospatial information as to the location of *SMILR* within HSVMSCs. Negative control samples showed no fluorescent signal, whereas SNORD3 fluorescent activity confirmed the nuclear

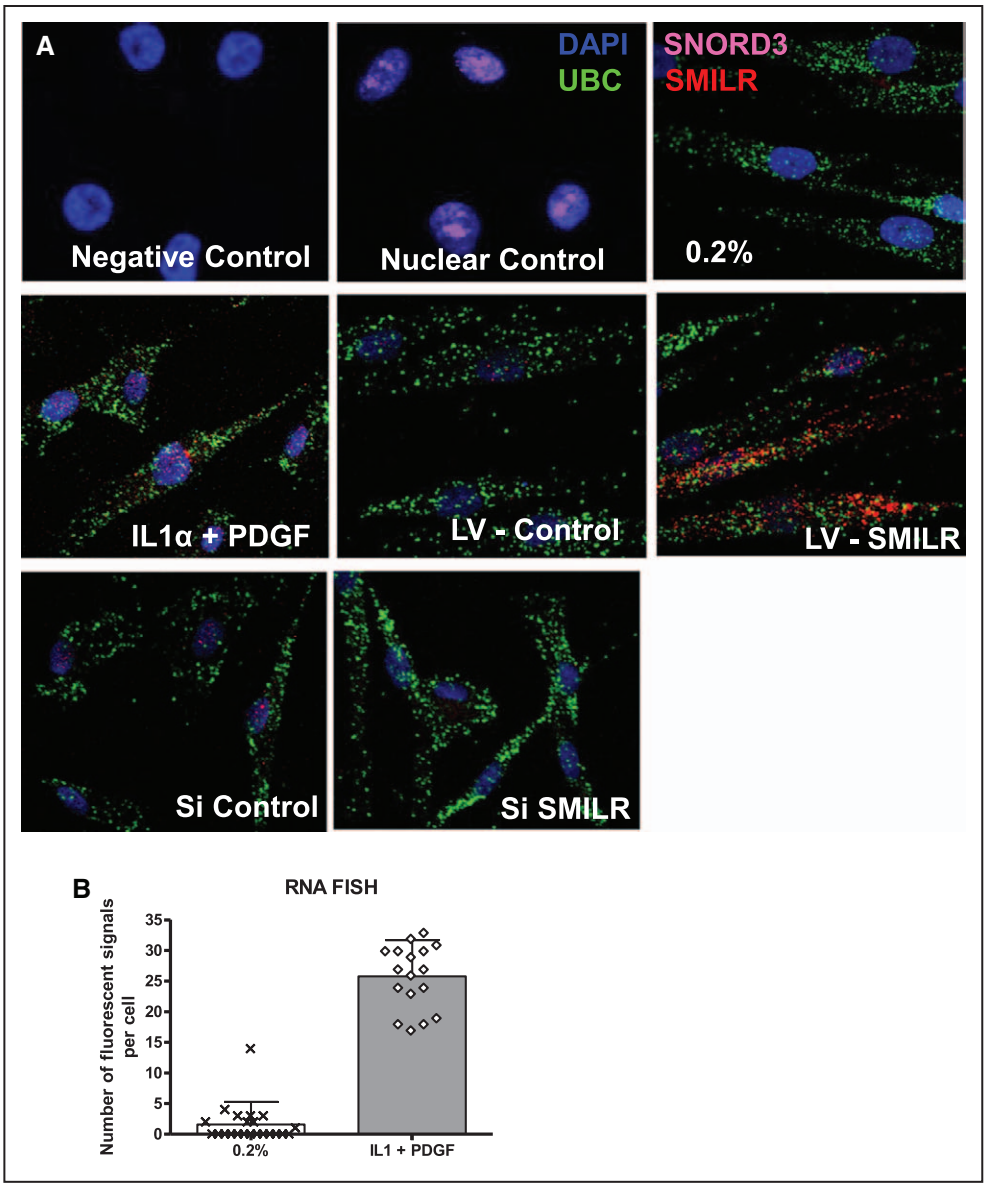

Figure 4. Localization of *SMILR*. **A**, RNA FISH analysis of *SMILR,* cytoplasmic *UBC* mRNA, and nuclear *SNORD3* RNA in HSVSMC. Magnification ×630 for all panels. UBC and *SNORD3* used for confirmation of cellular compartments. **B**, Quantification of lncRNA molecules per cell in indicated conditions. More than 5 images were selected at random from each condition, and at least 4 cells were counted in each image. DAPI indicates 4,6-diamidino-2-phenylindole-2-HCl; FISH, fluorescent in situ hybridization; HSVSMC, human saphenous vein–derived smooth muscle cell; IL1α, interleukin-1α; lncRNA, long noncoding RNA; LV, lentivirus; PDGF, platelet-derived growth factor; si, small interfering; UBC, ubiquitin U.

permeabilization of cells (Figure 4A). In the absence of growth factor and cytokine stimulation, HSVSMCs typically exhibited between 0 and 3 positive fluorescent signals corresponding to *SMILR* localization (Figure 4A). IL1α/PDGF treatment induced a marked increase in fluorescent signal within the nucleus and cytoplasm of HSVSMCs. Further specificity of the FISH probes was confirmed through the use of cells treated with either lentivirus containing *SMILR* or small interfering RNA (siRNA)–targeting *SMILR*. In each case, an increase and decrease in *SMILR* transcripts was observed (Figure 4A). Quantification of FISH samples is provided in Figure 4B. In the absence of stimulation, 2±3.6 *SMILR* molecules were observed. Following stimulation, 25±5 individual *SMILR* molecules were observed within the nucleus and cytoplasm (Figure 4B).

Identifying Upstream Mediators of *SMILR* Expression in HSVSMCs

It is well established that IL1α and PDGF work through distinct pathways leading to vascular cell activation. To assess the functional consequences of inhibition of these pathways on *SMILR* expression, selective pharmacological inhibitors AZD6244 (MEKK1) and SB 203580 (p38) were used (Figure 5A). Following 60 minutes of pretreatment with inhibitors, VSMCs were stimulated with IL1α/PDGF, and the expression of *SMILR* was determined at 24 hours. Pretreatment with AZD6244 (5, 10, or 15 μmol/L) prevented the induction of *SMILR* in response to PDGF and IL1α (Figure 5B), whereas inhibition of p38 with SB203580 induced a dose-dependent reduction in *SMILR* expression in response to PDGF and IL1α (Figure 5C).

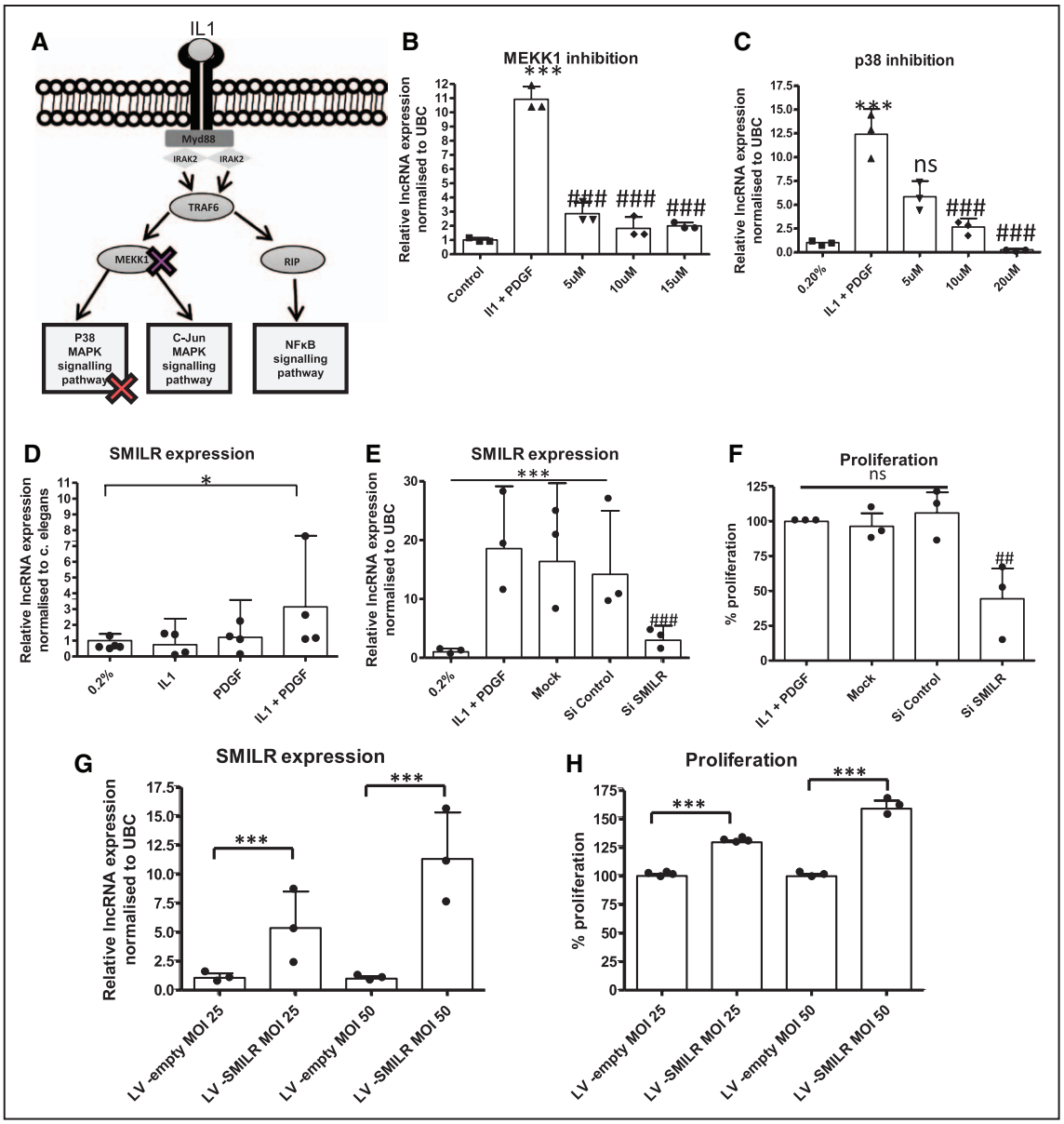

Figure 5. Functional regulation of *SMILR*. **A**, Schematic diagram showing specific sites of inhibition. HSVSMCs were pretreated for 60 minutes with the indicated concentration of the inhibitors. Following exposure to vehicle or 10 ng/mL IL1 or 20 nmol/L PDGF for 24 hours, expression of SMILR was determined by qRT-PCR. **B**, SMILR expression following MEKK1 inhibition. ***P<0.01 vs 0.2% media, ### P<0.001 vs IL1/PDGF treatment. Repeated-measures ANOVA (n=3). **C**, SMILR expression following p38 inhibition. Repeated-measures ANOVA. ***P<0.01 vs 0.2% media, ### P<0.001 vs IL1/PDGF treatment alone (n=3). **D**, SMILR expression in conditioned media from HSVSMCs cultured in 0.2%, IL1 or PDGF conditions. Unpaired t test. *P<0.05 vs 0.2% (n=4). **E**, Confirmation of the effect of siRNA targeting SMILR in HSVSMCs by using qRT-PCR (n=3). One-way ANOVA ***P<0.001 vs 0.2% control. ### P<0.001 vs IL1 + PDGF treatment. **F**, IL1/PDGF induced proliferation classed as 100% for analysis across patient samples, knockdown of *SMILR* inhibits EdU incorporation in HSVSMCs (n=3) One-way ANOVA vs Si control. ## P<0.01. **G**, qRT-PCR analysis of SMILR expression following infection with either an empty lentivirus (LV-E) or lentivirus containing *SMILR* sequence (LV-S) at an MOI of 25 (n=3) and MOI 50 (n=3) ***P<0.001 vs relevant empty control assessed via multiple-comparison ANOVA. ANOVA indicates analysis of variance; EdU, 5-ethynyl-2′-deoxyuridine; HSVSMC, human saphenous vein–derived smooth muscle cell; IL1α, interleukin-1α; lncRNA, long noncoding RNA; MAPK, mitogen-activated protein kinase; MOI, multiplicity of infection; ns, not significant; PDGF, platelet-derived growth factor; qRT-PCR, quantitative real-time polymerase chain reaction; Si, small interfering; siRNA, small interfering RNA; and UBC, ubiquitin.

IL1α/PDGF Treatment Induces the Release of *SMILR* Into Conditioned Media

miRNAs have been reported to be secreted from cells as a means of cell-to-cell communication.[26] To investigate whether HSVSMCs release *SMILR* as an indication of expression, we modified a method commonly used to evaluate miRNA expression.[27] Because no endogenous control was stably expressed across all conditions in this study, an exogenous control was added to monitor extraction efficiency and to normalize data. Consequently, total RNA from *C elegans* was used as a spike-in, and *ama-1* encoding polymerase II was chosen as a control for its high constitutive expression (see Methods). Interestingly, *SMILR* was detected at low levels in media from quiesced VSMCs and those stimulated by

either PDGF or IL1α, whereas conditioned media obtained from VSMC stimulated by combination contained significantly higher levels of *SMILR* (4.8±4.5–fold; Figure 5D), consistent with the increased intracellular expression of *SMILR* following costimulation of VSMC. Thus, treatment with PDGF and IL1α increased intracellular and released levels of *SMILR*.

In addition, we sought to identify if *SMILR* was encapsulated within exosomes or microvesicles. We used both ultracentrifugation, to remove cell debris, and an exosome isolation kit. Figure XIA and XIB in the online-only Data Supplement confirms the presence of microvesicles and exosomes by using Nanosight technology and the expression of the previously described miR-143 within the exosomes/microvesicles.[28] Our data highlighted the expression of *SMILR* restricted to exosome-free media (Figure IXC in the online-only Data Supplement) and the inability to detect *SMILR* expression in the exosome/microvesicle compartment using both techniques of isolation. This observation has been confirmed by agarose gel electrophoresis (Figure XID in the online-only Data Supplement). Primer melting curves are also shown in Figure XIE in the online-only Data Supplement. Our data confirm that *SMILR* is secreted into the media and located in a nonexosome/microvesicle fraction. This could possibly be through interaction with specific membrane channels but requires additional experimentation.

In addition, we examined the release of *SMILR* following lentiviral overexpression in IL1- and PDGF-treated cells. Lentiviral overexpression resulted in a 10-fold increase in *SMILR* RNA intracellularly. However, only a marginal (not significant) increase was observed within conditioned media analyzed from infected cells (Figure XIF in the online-only Data Supplement). When this media was transferred onto additional quiesced cells, no change in proliferation was detected (Figure XIG in the online-only Data Supplement). This may suggest that the release of *SMILR* is under a stringent control mechanism and simply increasing *SMILR* expression via a lentiviral approach is not sufficient to induce the additional release of this lncRNA from the cells. In addition, these cells were stimulated with IL1α and PDGF, which strongly enhances *SMILR* expression in VSMC. The secretory machinery may have been saturated with the high levels of lncRNA within the cytoplasm. This has previously been demonstrated with miRNA where high levels of miR, via overexpression with miRNA mimics, saturated the exportin-5 pathway of endogenous miRNAs with fatal consequences.[29,30]

Effect of Dicer Substrate siRNA–Mediated Knockdown of SMILR on HSVSMC Proliferation

We investigated the function of *SMILR* using dicer substrate siRNA (dsiRNA)–mediated knockdown and 5-ethynyl-2′-deoxyuridine incorporation. Forty-eight hours after stimulation, IL1α and PDGF treatment induced a 34±15% increase in VSMC proliferation in comparison with control (Figure XII in the online-only Data Supplement). dsiRNA *SMILR* caused 75±24% decrease in *SMILR* expression in comparison with dsi-control (Figure 5E). Following *SMILR* knockdown with dsiRNA, VSMC proliferation was reduced by 56±15% (Figure 5F). Results were confirmed through the use of a second dsiRNA targeting an alternative region of *SMILR* (Figure XIIIA and XIIIB in the online-only Data Supplement). No effect on the interferon pathway was observed via assessment of the response genes *OAS1* and *IRF7*, which have previously been linked to dsiRNA off-target effects[31] (Figure XIIIC and XIIID in the online-only Data Supplement).

In addition, the effect of *SMILR* overexpression on VSMC proliferation was investigated. VSMCs were infected with *SMILR* lentivirus or empty control for 24 hours before stimulation. Infection at a multiplicity of infection of 25 and 50 produced a 5.5±3.5– and 11.4±4.7–fold increase in *SMILR* expression in comparison with the empty control, with no apparent toxicity effects (Figure 5G). Overexpression produced a dose-dependent increase of 1.3±0.3–fold and 1.66±0.5–fold in VSMC proliferation, respectively (Figure 5H), confirming the knockdown data.

SMILR Expression Correlates With Other Proximal Genes

The expression of lincRNAs can correlate with the expression of adjacent genes and other RNAs within the genomic locale.[32] We therefore assessed the expression of genes and noncoding RNAs within 5 million base pairs of *SMILR*, from *COL14A1* on the forward strand to *FERIL6-AS1* on the reverse strand (Figure 6A) by using the RNA-seq data set (Figure 6B). Upregulation of *SMILR* was not associated with a widespread increase in transcriptional activity within the region (Figure 6B). However, similar changes in expression in response to VSMC stimulation were observed in 2 proximal transcripts (*HAS2* and *HAS2-AS1*). *SMILR* is located ≈750 kbp downstream of *HAS2* on the same (reverse) strand and ≈350 kbp from *ZHX2* and ≈750 kbp from *HAS2-AS1* on the opposite strand of chromosome 8 (Figure 6C). The upregulation of *HAS2* was accompanied by an increase in *HAS1* but not *HAS3* following dual stimulation (Figure 6D through 6F). Interestingly, IL1α and PDGF in combination had no effect on *HAS3* expression because IL1α and PDGF have opposing effects on *HAS3* expression (full graph with single stimulation, Figure XIIIE and XIIIF in the online-only Data Supplement). In addition to *SMILR*, upregulation of *HAS2-AS1* was evident following IL1α and PDGF treatment, but not *ZHX1* in the RNA-seq data (data not shown). This observation was validated by qRT-PCR (Figure 6G through 6I).

It has been previously shown that lncRNA can modulate the expression of nearby protein-coding genes. Thus, the expression of proximal genes *HAS2*, *ZHX2*, and *HAS2-AS1* was determined following *SMILR* knockdown. RNA interference–mediated knockdown of *SMILR* significantly altered levels of *HAS2* mRNA. However, no change in the *HAS2-AS1* lncRNA or the *ZHX2* gene was observed via qRT-PCR (Figure 6J through 6L). Results were confirmed by using a second siRNA-targeting *SMILR* (Figure XIIIG through XIIII in the online-only Data Supplement). In addition, no effect on *HAS1* or *HAS3* expression was observed while *SMILR* siRNA was used, indicating that the effect of *SMILR* knockdown is specific to *HAS2* and not all isoforms of *HAS* (Figure 6M and 6N).

In addition, knockdown of *HAS2-AS1* greatly reduced *HAS2* expression with no effect on *SMILR* expression (Figure

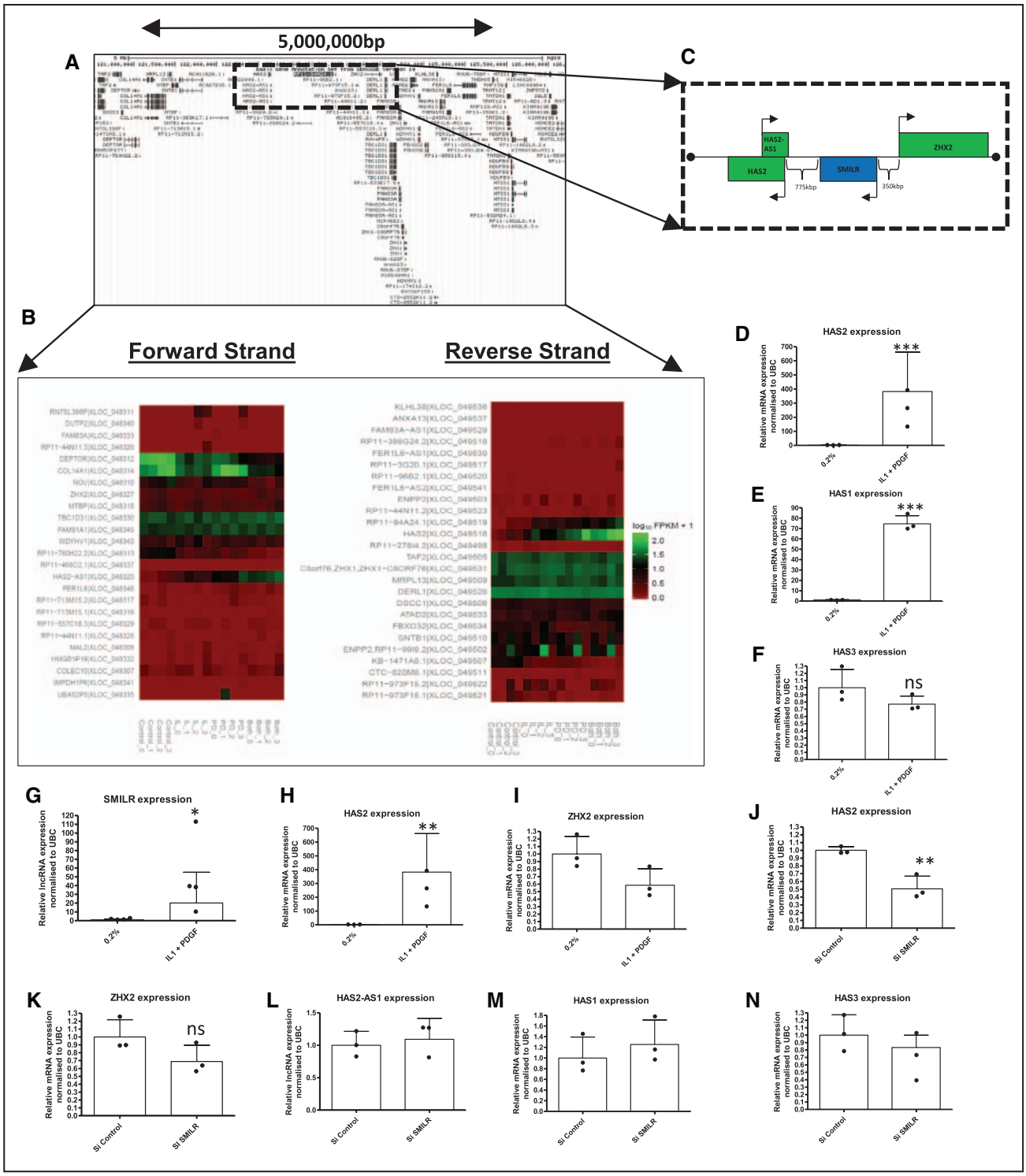

Figure 6. *SMILR* regulates proximal gene *HAS2* in chromosome 8. **A**, Schematic view of the 8q24.1 region showing lncRNAs and protein-coding genes over the 5 000 000-bp region from Ensemble. **B**, Regulation of protein-coding and noncoding genes within the selected region following IL1α and PDGF treatment; heatmap depicts expression of genes found with RNA-seq in 4 patient samples. **C**, Dotted line marks region containing *SMILR* lincRNA and closest protein-coding genes *HAS2* and *ZHX2*. **D**, Expression of proximal gene *HAS2* – modulated in the same manner as *SMILR* with IL1α and PDGF treatment (n=3). Unpaired *t* test: ***P<0.001 vs 0.2%. **E** and **F**, Additional HAS isoforms are differentially modulated by IL1 and PDGF (n=3). Unpaired *t* test: ***P<0.001 vs 0.2%. **G** through **I**, Validation of RNA-seq data for lncRNAs SMILR and HAS2-AS1 by qRT-PCR (n=3). *P<0.05 and **P<0.01 vs 0.2%, unpaired *t* test. **J**, Inhibition of *SMILR* expression via dsiRNA treatment significantly inhibits HAS2 expression determined by qRT-PCR **P<0.01 vs Si control. Unpaired *t* test (n=3). **K** through **N**, *SMILR* inhibition had no effect on proximal genes ZHX2 or HAS2-AS1 nor additional HAS isoforms, HAS1 or HAS3 (n=3). Unpaired *t* test. ANOVA indicates analysis of variance; dsiRNA, dicer substrate small interfering RNA; HSVSMC, human saphenous vein–derived smooth muscle cell; IL1α, interleukin-1α; lincRNA, intervening long noncoding RNA; lncRNA, long noncoding RNA; PDGF, platelet-derived growth factor; qRT-PCR, quantitative real-time polymerase chain reaction; Si, small interfering; and UBC, ubiquitin.

XIVA and XIVB in the online-only Data Supplement). However, the reverse experiment using *HAS2* knockdown did not affect the expression of *HAS2-AS1* or *SMILR* (Figure XIVC in the online-only Data Supplement). Finally, lentiviral-mediated overexpression did not affect *HAS1*, *HAS2*, *HAS3*, or *HAS2-AS1* expression (Figure XIVD through XIVG in the online-only Data Supplement).

SMILR Expression Is Dysregulated in Unstable Human Carotid Plaques

To investigate the importance of *SMILR* in human vascular pathologies, we assessed levels of *SMILR* in unstable atherosclerotic plaques. We used 2 established inflammatory ([^{18}F] fluorodeoxyglucose [FDG]) and calcification ([^{18}F]fluoride) positron emission tomography radiotracers to define prospectively portions of high-risk plaque[33–35] for RNA extraction. Plaque and relatively healthy adjacent sections of vessel were assessed from within individual patients (Table V in the online-only Data Supplement for patient characteristics). This is of key importance because it permits the assessment of noncoding RNA expression from within each micro environment (plaque versus nonplaque) from the 1 vessel. In comparison with quiescent adjacent tissue, portions of high-risk plaque showed higher uptake of both [^{18}F]FDG (maximum tissue-to-background ratio 1.81±0.21 versus 1.31±1.6) and [18F]fluoride (maximum tissue-to-background ratio 2.32±0.52 versus 1.31±0.43) indicating that plaques subjected to RNA analysis had enhanced rates of inflammation (Figure 7A through 7G for image examples and Figure 7H through 7K for graphs of tracer uptake). Because noncoding RNAs have not been assessed in a similar sample set before, we first confirmed whether expression of a panel of miRNAs associated with atherosclerosis processes were dysregulated.[36] As expected, inflammation-associated miRNAs 146a and 146b were significantly upregulated in unstable plaques in comparison with adjacent quiescent tissue, whereas miR-29 and miR-204, which are inversely associated with osteoblastogenesis and arterial calcification, were downregulated in mineralized regions of the atherosclerotic plaque.[37,38] In addition, we also found a downregulation of the miR-143/145 cluster, which is associated with SMC differentiation and aortic aneurysm formation,[39] an event that has previously been linked to osteogenic differentiation of SMC (Figure 7L). Thus expression of small noncoding RNAs (miRs) was associated with positron emission tomography/computed tomography-defined high-risk plaques. Therefore, we used the same cohort of samples to assess *SMILR*, *HAS2*, and *HAS2-AS1* levels. A 3.9±2.3–fold increase in *SMILR* expression was observed in high-risk plaques in comparison with adjacent stable regions of the carotid artery (Figure 7M). Intriguingly, we also observed an increased in *HAS2* (Figure 7N) but not *HAS2-AS1* (Figure 7O).

SMILR Is Detectable in Human Plasma and Correlates With Inflammatory C-Reactive Protein

Because of the release of *SMILR* into conditioned media from VSMC following stimulation with inflammatory mediators, we evaluated whether *SMILR* was detectable in stored samples from a cohort of men with varying metabolic dysfunction. These samples were ranked in order of the serological parameter C-reactive protein (CRP) levels into 3 groups: CRP <2, CRP 2 to 5, and CRP >5 mg/L representing broad tertiles of CRP. *SMILR* showed no difference in patients with CRP levels below 2 mg/L versus 2 to 5 mg/L. However, a significant increase in *SMILR* was observed when CRP concentrations were >5 mg/ml (0.008±0.006 for CRP <2 mg/L and 0.046±0.05 for CRP >5 mg/L; Figure 8A). Furthermore, a significant positive correlation was seen between *SMILR* and CRP (R^2=0.33, P<0.0001; Figure 8B). There was no correlation between *SMILR* and additional risk factors including age (P=0.66), blood pressure (P=0.12), BMI (P=0.14), or social deprivation status (P=0.11; Table VI in the online-only Data Supplement). Melting curves and gel products of *SMILR* primers in plasma are shown in Figure XV in the online-only Data Supplement. Further information regarding the statistical analysis of *SMILR* CRP correlation can be found in Figure XVI in the online-only Data Supplement.

Discussion

We have shown that stimulation of HSVSMCs with PDGF and IL1α increases expression of *SMILR*. This novel lincRNA increases cell proliferation, which may be linked to its ability to regulate the proximal gene *HAS2*. In a clinical setting, we found increased expression of *SMILR* in unstable atherosclerotic plaques suggesting an association with fundamentally important vascular pathologies linked to inflammation and VSMC proliferation. We also discovered that *SMILR* can be released from cells and is detectable in plasma from patients with enhanced inflammation and thus susceptibility to atherosclerosis. These findings support the growing body of evidence that noncoding RNAs can act as mediators to modulate disease pathways.

Recent advances in RNA sequencing have demonstrated that previously thought genome deserts are in fact pervasively transcribed and are populated by lncRNAs. The use of paired-end sequencing allowed the accurate alignment of reads to the human genome (GRCh37), the 93% alignment rate met quality standards for the RNA-seq technique[40] and ensured that our RNA-seq provided a high-quality profile of the HSVSMC transcriptome during quiescent and stimulated conditions. Notably, in comparison with control cells, protein-coding genes accounted for 3- to 4-fold greater abundance than lncRNAs. Our RNA-seq depth of 70 million reads was sufficient to identify lncRNAs within VSMC; however, it should be noted that greater read depths and the use of refined capture-sequencing technique would be beneficial to offer greater annotation of specific areas within the genome.

Analysis of the RNA-seq data pinpointed *SMILR* as an IL1α/PDGF–responsive lincRNA located on chromosome 8, 750 kbp from the closest protein-coding gene, on the same strand. This gene, *HAS2*, encodes an enzyme that synthesizes hyaluronic acid (HA), a critical component of the extracellular matrix that accumulates in human restenotic and atherosclerotic lesions.[41,42] Our results show that knockdown of *SMILR* reduces *HAS2* expression and VSMC proliferation. This mechanism of action is supported by a number of studies demonstrating that HA can enhance VSMC proliferation and

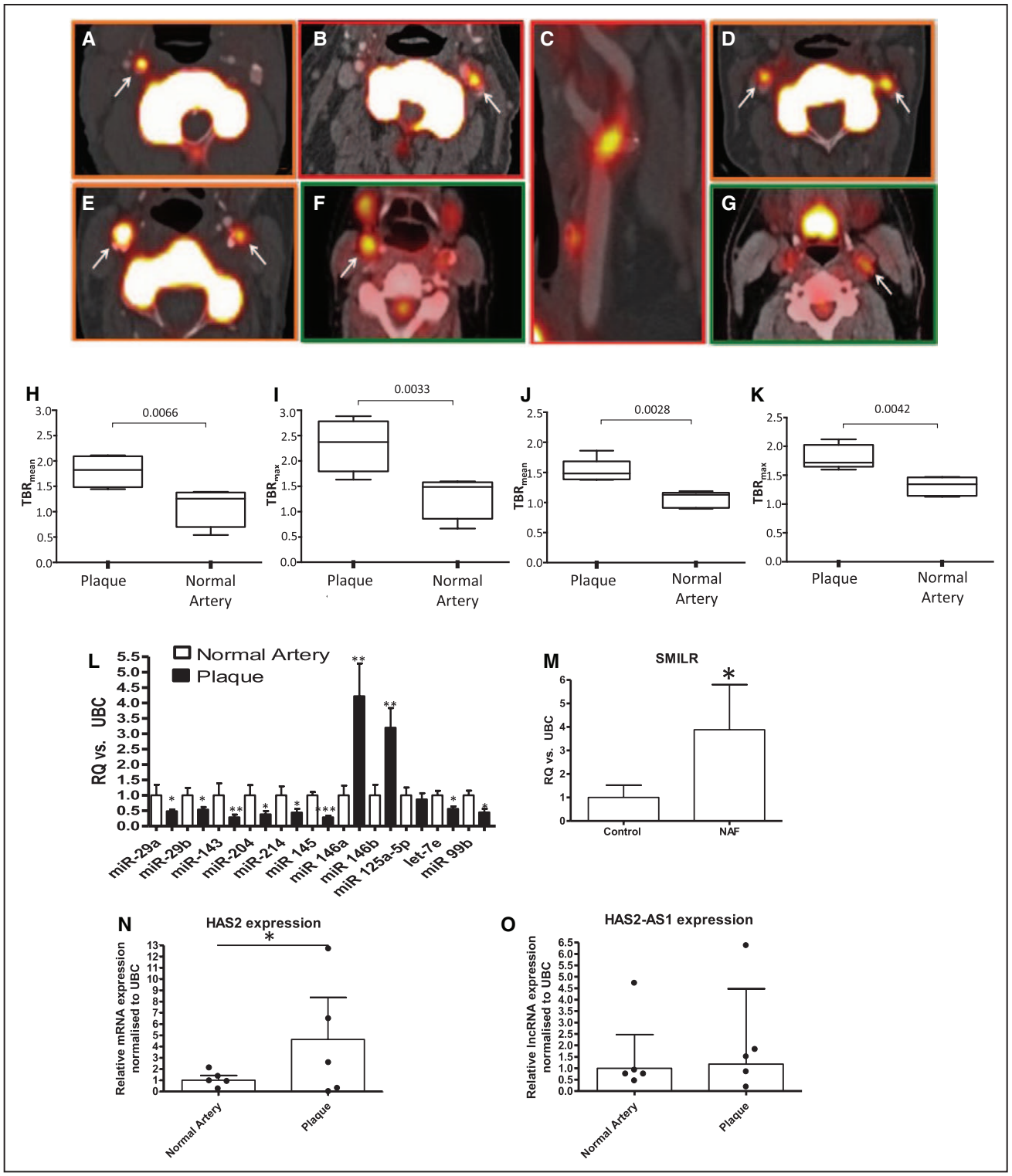

Figure 7. Uptake of [^{18}F]fluoride and [^{18}F]FDG within plaque and normal artery and changes in noncoding RNA expression within carotid plaques. Axial images demonstrating unilateral (**A**, **B**) or bilateral [^{18}F]fluoride carotid uptake (**D**, **E**). **C** is a multiplanar reformat of **B**. Axial images demonstrating [^{18}F]FDG carotid uptake (**F**, **G**). **H** shows the Siemens Biograph Clinical PET/CT system used for imaging. White arrows indicate carotid radioligand uptake. **H** through **K**, **L**, Uptake of tracer: MicroRNA profile of atherosclerotic plaque and paired healthy carotid controls (n=6) assessed by qRT-PCR (paired Student *t* test). Expression of *SMILR* (**M**), *HAS2* (**N**), and *HAS2-AS1*(**O**) within atherosclerotic plaque (n=5). Analyzed via qRT-PCR analysis, ***P<0.001, **P<0.01, and *P<0.05 assessed by paired Student *t* test. CT, computed tomography; [^{18}F]FDG, ^{18}F-fluorodeoxyglucose; PET, positron emission tomography; and qRT-PCR, quantitative real-time polymerase chain reaction.

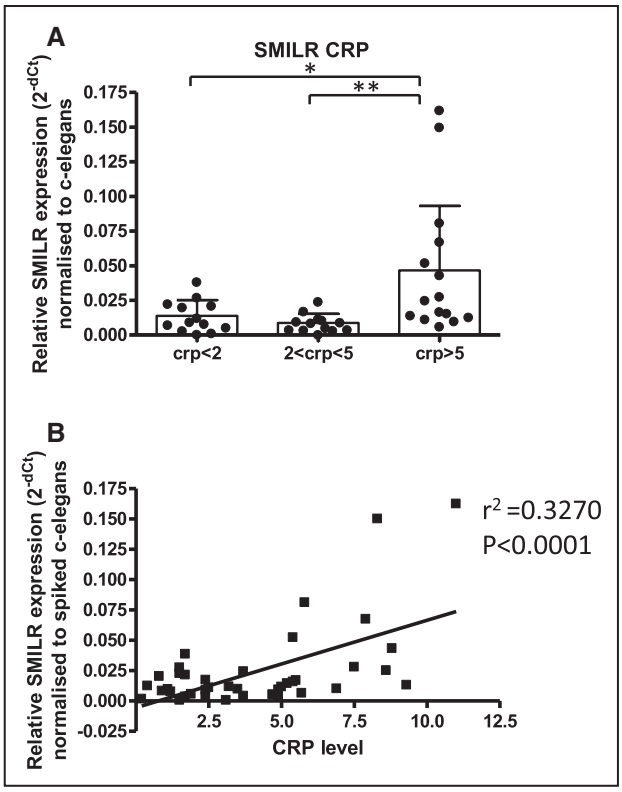

Figure 8. *SMILR* is detectable within plasma samples and correlates with patient CRP levels. **A**, *SMILR* expression is increased in patients with higher CRP levels (n=13 CRP<2; n=13 CRP2–5; and n=15 CRP>5; **P*<0.05, ***P*<0.01 via 1-way ANOVA). **B**, Correlation between *SMILR* expression and CRP levels (linear regression *P*<0.0001). CRP indicates C-reactive protein; lncRNA, long noncoding RNA; and UBC, ubiquitin.

migration.[43] Recent studies using transgenic mice with VSMC-specific overexpression of HA have found increased susceptibility to atherosclerosis[44] and enhanced neointima formation in response to cuff injury.[45] The ability of *SMILR* to specifically target *HAS2* with no effect on *HAS1* or *HAS3* allows a means of specifically altering *HAS2* expression, the main *HAS* isoform expressed and functioning in SMC pathology.[46]

lncRNAs can regulate other RNAs via a number of mechanisms,[47] including changes in chromatin signatures within their locus. For example, the *HOTAIR* lncRNA is capable of repressing transcription in *trans* across 40 kbp of the *HOXD* locus.[48] Thus *SMILR* may act as an enhancer or scaffold via interaction with the promoter region, and potentially other transcription factors of *HAS2*, to regulate expression following inflammatory cytokine stimulation. However, further detailed coimmunoprecipitation or site-directed mutagenesis studies would be required to demonstrate whether *SMILR* participates in transcription factor complexes with NF-κβ or other transcription factors. Previous work has found that *HAS2* is regulated by an additional lncRNA, *HAS2-AS1*.[49] Interestingly, our RNA-seq data show *HAS2-AS1* expression was also upregulated by PDGF treatment alone and in combination with IL1α. However, knockdown of *SMILR* did not alter *HAS2-AS1* expression. lncRNA *HAS2-AS1* modulates chromatin structures around the gene to allow more efficient binding of the RNA polymerase 2, and enhanced *HAS2* gene expression.[49] This suggests both *SMILR* and *HAS2-AS1* can regulate *HAS2* by independent mechanisms. Interestingly, knockdown of HAS2 did not affect either *SMILR* or *HAS2-AS1* expression, indicating that the expression of these lncRNAs is not directly linked to *HAS2* expression.

The composition of extracellular matrix assists in the determination of the stability of the atherosclerotic plaques, the phenotype of cells within it and the volume of neointima. During the progression of atherosclerosis, VSMCs are exposed to a plethora of signaling molecules, including inflammatory cytokines. Using the clinical gold-standard methods of [^{18}F]FDG and [^{18}F]fluoride positron emission tomography/computed tomography imaging to identify inflamed, necrotic, and mineralizing atherosclerotic plaque,[33,34] our results indicate that miRs 29, 143, 145, 146, and 204 are differentially expressed in unstable regions of atherosclerotic plaques. These miRs have previously been linked to VSMC differentiation, inflammatory cell signaling,[50] and VSMC calcification.[51] The strong association and colocalization of *SMILR* with this classical miRNA profile and focal [^{18}F]FDG and [^{18}F]fluoride uptake within atherosclerotic plaque suggests that *SMILR* may play a role in atherosclerosis through inflammatory and proliferative pathways. In keeping with our results showing *HAS2* regulation by *SMILR*, HA content has been shown to reflect the progression of atherosclerotic disease and promotes vessel wall thickening.[52] Indeed, HA has been implicated in the recruitment of inflammatory cells, known to play a prominent role in the initiation and progression of atherosclerotic lesion to an unstable plaque phenotype.

Our results demonstrate that *SMILR* is upregulated by a combination of PDGF and IL1α in VSMCs but not endothelial cells, suggesting that modulation of *SMILR* could specifically alter VSMC proliferation without detrimental effects on vessel reendothelialization. If this is the case, it would provide a suitable candidate to improve antiproliferative therapies because current pharmacological agents target cell proliferation in a non–cell-specific manner, events that can lead to late stent thrombosis.[53]

The ability to identify confidently a plaque, or patient, at particular risk of a major adverse cardiovascular event (ie, plaque rupture) remains an important goal of cardiovascular research. Long RNAs, both mRNA and noncoding RNA, have been previously shown to be stable in vivo for up to 3 weeks.[54] As such, the search for prognostic biomarkers has greatly increased in recent years. *SMILR* was expressed in both the nucleus and cytoplasm of cells following stimulation and was released into the media. It will be important to determine whether the cytoplasmic copies induce functional effects, such as regulation of gene expression through posttranslational mechanisms or if they are simply being processed for release. Dual transcriptional functions of lncRNAs have been shown previously,[55] but to date no reports of a single lncRNA affecting both transcription and translation have been published. The release of *SMILR* could affect function in neighboring cells, particularly in a vascular injury setting where phenotypic switching of VSMCs occurs in distinct areas of the vessel wall. In support of this theory, it has been shown that miR-143/145 can be transferred from VSMC into endothelial cells.[56] This transfer produced physiological effects

within endothelial cells, including modulation of angiogenesis. We also found that *SMILR* could be detected in the plasma of patients with higher CRP levels indicative of chronic low-grade inflammation. In light of our studies, we propose that this release could be attributable to the increased levels of *SMILR* in the diseased vasculature, although delineating whether plasma *SMILR* is simply a by-product of increased intracellular levels or is functionally active in disease pathology is difficult to definitely demonstrate. However, circulating levels of miR 143 and 145 are associated with in-stent restenosis and, as such, have been proposed as biomarkers.[57] The correlation of *SMILR* and high CRP further supports its expression in low-grade chronic inflammatory settings, and proliferative settings, as well. Further large clinical cohorts will be required to ascertain if *SMILR* has prognostic potential in inflammatory vascular disease and, if so, whether it provides enhanced prognostic value over current biomarkers.

Vessel renarrowing after surgical intervention and atherosclerosis remain significant clinical problems, and HA/*HAS2*/*SMILR* have emerged as key components of these pathological processes. Administration of an siRNA targeting *SMILR* could be used to prevent renarrowing after surgical intervention for acute coronary syndrome. The use of siRNAs has been proven to be effective in phase I clinical trials. Davis et al[58] recently showed a dose-dependent increase of siRNA delivered via nanoparticles and observed a reduction in the specific mRNA target. However, we must remain cautious, because early clinical trials in the setting of vein graft failure suggested that antisense oligonucleotides directed against E2F (edifoligide) were promising for the treatment of vein graft failure and atherosclerosis, but the subsequent phase 3 Project of Ex Vivo Vein Graft Engineering via Transfection IV (PREVENT IV) study yielded largely disappointing results.[59] However, these studies do demonstrate that the surgical setting of coronary artery bypass grafting provides the ideal clinical setting to evaluate the clinical efficacy of these targets by gene therapy, given that the vein can be transduced ex vivo at the time of surgery. Administration of siRNA directly to the vessel would obviate the need to administer siRNA systemically and thus reduce the possibility of off-target effects. Unfortunately, there are no clear homologues of *SMILR* in the mouse. It would, however, be important to determine whether other preclinical models of human vascular disease contain *SMILR* homologues, once this information becomes available.

Taken together, these observations broaden our awareness of the complex interplay between lncRNA and protein-coding genes. The emergence of lncRNAs as regulators of gene expression will undoubtedly alter our understanding of the complex regulation network of pathological VSMC proliferation in vascular disease and may provide a means to specifically target VSMC or identify patients at risk of major adverse vascular outcomes.

Acknowledgments

We thank N. Britton and G. Aitchison for technical assistance.

Sources of Funding

This work is supported by the British Heart Foundation (Program grant: RG/09/005/27915 and FS11/12/28673). Dr Ballantyne is supported by the British Heart Foundation PhD Studentship (FS/12/66/30003) and Dr Baker is supported by the British Heart Foundation Chair of Translational Cardiovascular Sciences (CH/11/2/28733). Clinical PET/CT studies and Dr Vesey were funded by the British Heart Foundation (PG/12/8/29371). Drs Dweck and Newby are supported by the British Heart Foundation (FS/14/78/31020 and CH/09/002). Dr Newby is the recipient of a Wellcome Trust Senior Investigator Award (WT103782AIA). The Wellcome Trust Clinical Research Facility and the Clinical Research Imaging Center are supported by NHS Research Scotland (NRS) through NHS Lothian.

Disclosures

None.

References

1. Marx SO, Totary-Jain H, Marks AR. Vascular smooth muscle cell proliferation in restenosis. *Circ Cardiovasc Interv*. 2011;4:104–111. doi: 10.1161/CIRCINTERVENTIONS.110.957332.
2. Ghouri N, Purves D, McConnachie A, Wilson J, Gill JM, Sattar N. Lower cardiorespiratory fitness contributes to increased insulin resistance and fasting glycaemia in middle-aged South Asian compared with European men living in the UK. *Diabetologia*. 2013;56:2238–2249. doi: 10.1007/s00125-013-2969-y.
3. Gomez D, Owens GK. Smooth muscle cell phenotypic switching in atherosclerosis. *Cardiovasc Res*. 2012;95:156–164. doi: 10.1093/cvr/cvs115.
4. Alexander MR, Owens GK. Epigenetic control of smooth muscle cell differentiation and phenotypic switching in vascular development and disease. *Annu Rev Physiol*. 2012;74:13–40. doi: 10.1146/annurev-physiol-012110-142315.
5. Schermuly RT, Dony E, Ghofrani HA, Pullamsetti S, Savai R, Roth M, Sydykov A, Lai YJ, Weissmann N, Seeger W, Grimminger F. Reversal of experimental pulmonary hypertension by PDGF inhibition. *J Clin Invest*. 2005;115:2811–2821. doi: 10.1172/JCI24838.
6. Rectenwald JE, Moldawer LL, Huber TS, Seeger JM, Ozaki CK. Direct evidence for cytokine involvement in neointimal hyperplasia. *Circulation*. 2000;102:1697–1702.
7. Dardik A, Yamashita A, Aziz F, Asada H, Sumpio BE. Shear stress-stimulated endothelial cells induce smooth muscle cell chemotaxis via platelet-derived growth factor-BB and interleukin-1alpha. *J Vasc Surg*. 2005;41:321–331. doi: 10.1016/j.jvs.2004.11.016.
8. Ferns GA, Raines EW, Sprugel KH, Motani AS, Reidy MA, Ross R. Inhibition of neointimal smooth muscle accumulation after angioplasty by an antibody to PDGF. *Science*. 1991;253:1129–1132.
9. Guan S, Tang Q, Liu W, Zhu R, Li B. Nobiletin Inhibits PDGF-BB-induced vascular smooth muscle cell proliferation and migration and attenuates neointimal hyperplasia in a rat carotid artery injury model. *Drug Dev Res*. 2014;75:489–496. doi: 10.1002/ddr.21230.
10. Johnson JL, Dwivedi A, Somerville M, George SJ, Newby AC. Matrix metalloproteinase (MMP)-3 activates MMP-9 mediated vascular smooth muscle cell migration and neointima formation in mice. *Arterioscler Thromb Vasc Biol*. 2011;31:e35–e44. doi: 10.1161/ATVBAHA.111.225623.
11. Elgar G, Vavouri T. Tuning in to the signals: noncoding sequence conservation in vertebrate genomes. *Trends Genet*. 2008;24:344–352. doi: 10.1016/j.tig.2008.04.005.
12. Salic K, De Windt LJ. MicroRNAs as biomarkers for myocardial infarction. *Curr Atheroscler Rep*. 2012;14:193–200. doi: 10.1007/s11883-012-0238-z.
13. Jiang Y, Wang HY, Li Y, Guo SH, Zhang L, Cai JH, Cao HM, Wang CY, Wang H, Liu L. Peripheral blood miRNAs as a biomarker for chronic cardiovascular diseases. *Sci Rep*. 2014;4:5026. doi: 10.1038/srep05026.
14. Jiang Y, Wang HY, Cao HM, Wang CY, Zhang L, Wang H, Liu L, Li Y, Cai JH. Peripheral blood miRNAs as a biomarker for chronic cardiovascular diseases. *Sci Rep*. 2014;4.
15. Kaushik K, Leonard VE, Kv S, Lalwani MK, Jalali S, Patowary A, Joshi A, Scaria V, Sivasubbu S. Dynamic expression of long non-coding RNAs (lncRNAs) in adult zebrafish. *PLoS One*. 2013;8:e83616.
16. Liu JY, Yao J, Li XM, Song YC, Wang XQ, Li YJ, Yan B, Jiang Q. Pathogenic role of lncRNA-MALAT1 in endothelial cell dysfunction in diabetes mellitus. *Cell Death Dis*. 2014;5:e1506. doi: 10.1038/cddis.2014.466.
17. Bell RD, Long X, Lin M, Bergmann JH, Nanda V, Cowan SL, Zhou Q, Han Y, Spector DL, Zheng D, Miano JM. Identification and initial

functional characterization of a human vascular cell-enriched long noncoding RNA. *Arterioscler Thromb Vasc Biol*. 2014;34:1249–1259. doi: 10.1161/ATVBAHA.114.303240.
18. Jaffe EA, Nachman RL, Becker CG, Minick CR. Culture of human endothelial cells derived from umbilical veins. Identification by morphologic and immunologic criteria. *J Clin Invest*. 1973;52:2745–2756. doi: 10.1172/JCI107470.
19. Southgate KM, Davies M, Booth RF, Newby AC. Involvement of extracellular-matrix-degrading metalloproteinases in rabbit aortic smooth-muscle cell proliferation. *Biochem J*. 1992;288(pt 1):93–99.
20. Dodt M, Roehr JT, Ahmed R, Dieterich C. FLEXBAR-flexible barcode and adapter processing for next-generation sequencing platforms. *Biology (Basel)*. 2012;1:895–905. doi: 10.3390/biology1030895.
21. Kim D, Pertea G, Trapnell C, Pimentel H, Kelley R, Salzberg SL. TopHat2: accurate alignment of transcriptomes in the presence of insertions, deletions and gene fusions. *Genome Biol*. 2013;14:R36. doi: 10.1186/gb-2013-14-4-r36.
22. Trapnell C, Williams BA, Pertea G, Mortazavi A, Kwan G, van Baren MJ, Salzberg SL, Wold BJ, Pachter L. Transcript assembly and quantification by RNA-Seq reveals unannotated transcripts and isoform switching during cell differentiation. *Nat Biotechnol*. 2010;28:511–515. doi: 10.1038/nbt.1621.
23. Trapnell C, Hendrickson DG, Sauvageau M, Goff L, Rinn JL, Pachter L. Differential analysis of gene regulation at transcript resolution with RNA-seq. *Nat Biotechnol*. 2013;31:46–53. doi: 10.1038/nbt.2450.
24. Livak KJ, Schmittgen TD. Analysis of relative gene expression data using real-time quantitative PCR and the 2(-Delta Delta C(T)) Method. *Methods*. 2001;25:402–408. doi: 10.1006/meth.2001.1262.
25. Billings FTt, Balaguer JM, C Y, Wright P, Petracek MR, Byrne JG, Brown NJ, Pretorius M. Comparative effects of angiotensin receptor blockade and ACE inhibition on the fibrinolytic and inflammatory responses to cardiopulmonary bypass. Clin Pharmacol Ther. 2012;91:1065–1073.
26. Glynn CL, Khan S, Kerin MJ, Dwyer RM. Isolation of secreted microRNAs (miRNAs) from cell-conditioned media. *Microrna*. 2013;2:14–19.
27. Morley-Smith AC, Mills A, Jacobs S, Meyns B, Rega F, Simon AR, Pepper JR, Lyon AR, Thum T. Circulating microRNAs for predicting and monitoring response to mechanical circulatory support from a left ventricular assist device. *Eur J Heart Fail*. 2014;16:871–879. doi: 10.1002/ejhf.116.
28. Deng L, Blanco FJ, Stevens H, Lu R, Caudrillier A, McBride M, McClure JD, Grant J, Thomas M, Frid M, Stenmark K, White K, Seto AG, Morrell NW, Bradshaw AC, MacLean MR, Baker AH. MicroRNA-143 activation regulates smooth muscle and endothelial cell crosstalk in pulmonary arterial hypertension. *Circ Res*. 2015;117:870–883. doi: 10.1161/CIRCRESAHA.115.306806.
29. Soifer HS, Rossi JJ, Saetrom P. MicroRNAs in disease and potential therapeutic applications. *Mol Ther*. 2007;15:2070–2079. doi: 10.1038/sj.mt.6300311.
30. Grimm D, Streetz KL, Jopling CL, Storm TA, Pandey K, Davis CR, Marion P, Salazar F, Kay MA. Fatality in mice due to oversaturation of cellular microRNA/short hairpin RNA pathways. *Nature*. 2006;441:537–541. doi: 10.1038/nature04791.
31. Karpala AJ, Doran TJ, Bean AG. Immune responses to dsRNA: implications for gene silencing technologies. *Immunol Cell Biol*. 2005;83:211–216. doi: 10.1111/j.1440-1711.2005.01331.x.
32. Wang KC, Chang HY. Molecular mechanisms of long noncoding RNAs. *Mol Cell*. 2011;43:904–914. doi: 10.1016/j.molcel.2011.08.018.
33. Rudd JH, Warburton EA, Fryer TD, Jones HA, Clark JC, Antoun N, Johnström P, Davenport AP, Kirkpatrick PJ, Arch BN, Pickard JD, Weissberg PL. Imaging atherosclerotic plaque inflammation with [18F]-fluorodeoxyglucose positron emission tomography. *Circulation*. 2002;105:2708–2711.
34. Joshi NV, Vesey AT, Williams MC, Shah AS, Calvert PA, Craighead FH, Yeoh SE, Wallace W, Salter D, Fletcher AM, van Beek EJ, Flapan AD, Uren NG, Behan MW, Cruden NL, Mills NL, Fox KA, Rudd JH, Dweck MR, Newby DE. 18F-fluoride positron emission tomography for identification of ruptured and high-risk coronary atherosclerotic plaques: a prospective clinical trial. *Lancet*. 2014;383:705–713. doi: 10.1016/S0140-6736(13)61754-7.
35. Vesey AT, Irkle A, Lewis DY, Skepper JN, Bird JLE, Dweck MR, Joshi FR, Gallagher FA, Warburton EA, Bennett MR, Brindle KM, Newby DE, Rudd JH, Davenport AP. YY Identifying active vascular microcalcification by F-18-Sodium fluoride positron emission tomography. *Brit J Surg*. 2015;102:5-5.
36. Raitoharju E, Lyytikäinen LP, Levula M, Oksala N, Mennander A, Tarkka M, Klopp N, Illig T, Kähönen M, Karhunen PJ, Laaksonen R, Lehtimäki T. miR-21, miR-210, miR-34a, and miR-146a/b are up-regulated in human atherosclerotic plaques in the Tampere Vascular Study. *Atherosclerosis*. 2011;219:211–217. doi: 10.1016/j.atherosclerosis.2011.07.020.
37. Du Y, Gao C, Liu Z, Wang L, Liu B, He F, Zhang T, Wang Y, Wang X, Xu M, Luo GZ, Zhu Y, Xu Q, Wang X, Kong W. Upregulation of a disintegrin and metalloproteinase with thrombospondin motifs-7 by miR-29 repression mediates vascular smooth muscle calcification. *Arterioscler Thromb Vasc Biol*. 2012;32:2580–2588. doi: 10.1161/ATVBAHA.112.300206.
38. Cui RR, Li SJ, Liu LJ, Yi L, Liang QH, Zhu X, Liu GY, Liu Y, Wu SS, Liao XB, Yuan LQ, Mao DA, Liao EY. MicroRNA-204 regulates vascular smooth muscle cell calcification in vitro and in vivo. *Cardiovasc Res*. 2012;96:320–329. doi: 10.1093/cvr/cvs258.
39. Elia L, Quintavalle M, Zhang J, Contu R, Cossu L, Latronico MV, Peterson KL, Indolfi C, Catalucci D, Chen J, Courtneidge SA, Condorelli G. The knockout of miR-143 and -145 alters smooth muscle cell maintenance and vascular homeostasis in mice: correlates with human disease. *Cell Death Differ*. 2009;16:1590–1598. doi: 10.1038/cdd.2009.153.
40. Mortazavi A, Williams BA, McCue K, Schaeffer L, Wold B. Mapping and quantifying mammalian transcriptomes by RNA-Seq. *Nat Methods*. 2008;5:621–628. doi: 10.1038/nmeth.1226.
41. Papakonstantinou E, Roth M, Block LH, Mirtsou-Fidani V, Argiriadis P, Karakiulakis G. The differential distribution of hyaluronic acid in the layers of human atheromatic aortas is associated with vascular smooth muscle cell proliferation and migration. *Atherosclerosis*. 1998;138:79–89.
42. Riessen R, Wight TN, Pastore C, Henley C, Isner JM. Distribution of hyaluronan during extracellular matrix remodeling in human restenotic arteries and balloon-injured rat carotid arteries. *Circulation*. 1996;93:1141–1147.
43. Papakonstantinou E, Karakiulakis G, Roth M, Block LH. Platelet-derived growth factor stimulates the secretion of hyaluronic acid by proliferating human vascular smooth muscle cells. *Proc Natl Acad Sci USA*. 1995;92:9881–9885.
44. Chai S, Chai Q, Danielsen CC, Hjorth P, Nyengaard JR, Ledet T, Yamaguchi Y, Rasmussen LM, Wogensen L. Overexpression of hyaluronan in the tunica media promotes the development of atherosclerosis. *Circ Res*. 2005;96:583–591. doi: 10.1161/01.RES.0000158963.37132.8b.
45. Kashima Y, Takahashi M, Shiba Y, Itano N, Izawa A, Koyama J, Nakayama J, Taniguchi S, Kimata K, Ikeda U. Crucial role of hyaluronan in neointimal formation after vascular injury. *PLoS One*. 2013;8:e58760. doi: 10.1371/journal.pone.0058760.
46. van den Boom M, Sarbia M, von Wnuck Lipinski K, Mann P, Meyer-Kirchrath J, Rauch BH, Grabitz K, Levkau B, Schrör K, Fischer JW. Differential regulation of hyaluronic acid synthase isoforms in human saphenous vein smooth muscle cells: possible implications for vein graft stenosis. *Circ Res*. 2006;98:36–44. doi: 10.1161/01.RES.0000199263.67107.c0.
47. Geisler S, Coller J. RNA in unexpected places: long non-coding RNA functions in diverse cellular contexts. *Nat Rev Mol Cell Biol*. 2013;14:699–712. doi: 10.1038/nrm3679.
48. Rinn JL, Kertesz M, Wang JK, Squazzo SL, Xu X, Brugmann SA, Goodnough LH, Helms JA, Farnham PJ, Segal E, Chang HY. Functional demarcation of active and silent chromatin domains in human HOX loci by noncoding RNAs. *Cell*. 2007;129:1311–1323. doi: 10.1016/j.cell.2007.05.022.
49. Vigetti D, Deleonibus S, Moretto P, Bowen T, Fischer JW, Grandoch M, Oberhuber A, Love DC, Hanover JA, Cinquetti R, Karousou E, Viola M, D'Angelo ML, Hascall VC, De Luca G, Passi A. Natural antisense transcript for hyaluronan synthase 2 (HAS2-AS1) induces transcription of HAS2 via protein O-GlcNAcylation. *J Biol Chem*. 2014;289:28816–28826. doi: 10.1074/jbc.M114.597401.
50. Taganov KD, Boldin MP, Chang KJ, Baltimore D. NF-kappaB-dependent induction of microRNA miR-146, an inhibitor targeted to signaling proteins of innate immune responses. *Proc Natl Acad Sci USA*. 2006;103:12481–12486. doi: 10.1073/pnas.0605298103.
51. Du Y, Gao C, Liu Z, Wang L, Liu B, He F, Zhang T, Wang Y, Wang X, Xu M, Luo GZ, Zhu Y, Xu Q, Wang X, Kong W. Upregulation of a disintegrin and metalloproteinase with thrombospondin motifs-7 by miR-29 repression mediates vascular smooth muscle calcification. *Arterioscler Thromb Vasc Biol*. 2012;32:2580–2588. doi: 10.1161/ATVBAHA.112.300206.
52. Johnson JL. Matrix metalloproteinases: influence on smooth muscle cells and atherosclerotic plaque stability. *Expert Rev Cardiovasc Ther*. 2007;5:265–282. doi: 10.1586/14779072.5.2.265.
53. Lemesle G, Maluenda G, Collins SD, Waksman R. Drug-eluting stents: issues of late stent thrombosis. *Cardiol Clin*. 2010;28:97–105. doi: 10.1016/j.ccl.2009.09.003.
54. Pinel K, Lacoste J, Plane G, Ventura M, Couillaud F. Long-term *in vivo* imaging of translated RNAs for gene therapy. *Gene Ther*. 2014;21:434–439. doi: 10.1038/gt.2013.89.

55. Vance KW, Sansom SN, Lee S, Chalei V, Kong L, Cooper SE, Oliver PL, Ponting CP. The long non-coding RNA Paupar regulates the expression of both local and distal genes. *EMBO J*. 2014;33:296–311. doi: 10.1002/embj.201386225.
56. Climent M, Quintavalle M, Miragoli M, Chen J, Condorelli G, Elia L. TGFβ triggers miR-143/145 transfer from smooth muscle cells to endothelial cells, thereby modulating vessel stabilization. *Circ Res*. 2015;116:1753–1764. doi: 10.1161/CIRCRESAHA.116.305178.
57. He M, Gong Y, Shi J, Pan Z, Zou H, Sun D, Tu X, Tan X, Li J, Li W, Liu B, Xue J, Sheng L, Xiu C, Yang N, Xue H, Ding X, Yu C, Li Y. Plasma microRNAs as potential noninvasive biomarkers for in-stent restenosis. *PLoS One*. 2014;9:e112043. doi: 10.1371/journal.pone.0112043.
58. Davis ME, Zuckerman JE, Choi CH, Seligson D, Tolcher A, Alabi CA, Yen Y, Heidel JD, Ribas A. Evidence of RNAi in humans from systemically administered siRNA via targeted nanoparticles. *Nature*. 2010;464:1067–1070. doi: 10.1038/nature08956.
59. Hess CN, Lopes RD, Gibson CM, Hager R, Wojdyla DM, Englum BR, Mack MJ, Califf RM, Kouchoukos NT, Peterson ED, Alexander JH. Saphenous vein graft failure after coronary artery bypass surgery: insights from PREVENT IV. *Circulation*. 2014;130:1445–1451. doi: 10.1161/CIRCULATIONAHA.113.008193.

CLINICAL PERSPECTIVE

Long noncoding RNAs (lncRNAs) are a relatively new class of discovered RNA molecules that possess important regulatory functions. The rapidly expanding catalogue of lncRNAs holds promise that, in the near future, lncRNAs might become relevant to vascular disease clinically as possible biomarkers of cardiovascular events and for targeted treatment of disease. Our work indicates that dysregulation of key lncRNAs may have profound implications in regulating vascular smooth muscle cell function. In addition, we detected the release of this lncRNA in plasma samples and correlated with inflammatory C-reactive protein levels, highlighting new methods and possibilities for improved detection. The emergence of lncRNAs as regulators of gene expression and vascular function will undoubtedly alter our understanding of the complex regulation network of cell function underpinning clinical vascular disease.

Smooth Muscle Enriched Long Noncoding RNA (*SMILR*) Regulates Cell Proliferation

Margaret D. Ballantyne, Karine Pinel, Rachel Dakin, Alex T. Vesey, Louise Diver, Ruth Mackenzie, Raquel Garcia, Paul Welsh, Naveed Sattar, Graham Hamilton, Nikhil Joshi, Marc R. Dweck, Joseph M. Miano, Martin W. McBride, David E. Newby, Robert A. McDonald and Andrew H. Baker

Circulation. 2016;133:2050-2065; originally published online April 6, 2016;
doi: 10.1161/CIRCULATIONAHA.115.021019
Circulation is published by the American Heart Association, 7272 Greenville Avenue, Dallas, TX 75231

Print ISSN: 0009-7322. Online ISSN: 1524-4539

SUPPLEMENTAL MATERIAL

Supplemental Methods

Tissue and Cell culture

Endothelial media supplemented 20% FCS (Life Technologies, Paisley, UK). HSVSMC media supplemented with 15% foetal bovine serum (FBS) (PAA laboratories, Yeovil, UK), 2 mM L-Glutamine (Invitrogen, Paisley, UK) 50 µg/ml penicillin (Invitrogen) and 50 µg/mL streptomycin (Invitrogen). All cells were used between passages 3-5.

HSVSMC BrdU and EdU Incorporation assay

HSVSMC proliferation was quantified using a DNA bromodeoxyuride (BrdU) incorporation assay (Millipore, Watford, UK), or EdU according to the manufacturer's instructions. Briefly, cells were plated and quiesced in 0.2% FCS media for 48 h prior to stimulation. Cells were stimulated with either 10 ng/mL IL1α, 20 ng/mL PDGF or a combination of both for the stated times. For BrdU experiments, 6 h after stimulation cells were incubated with BrdU and for EdU experiments EdU was added at the point of stimulation for the remaining time to allow cell proliferation. BrdU: after removing the culture medium, the cells were fixed followed by incubation with anti-BrdU antibody which binds the incorporated DNA. After adding the substrate solution, the immune complexes were detected using a plate reader set at dual wavelength of 450/550 nm, Victor (Perkin Elmer, Waltham, USA). EdU: following stimulation, cellular RNA was extracted as described earlier or fixed in 70% ethanol for EdU FACs analysis. EdU incorporation was quantified using Click-it EdU Proliferation assay with an Alexa Fluor 594 antibody according to the manufacturer's protocol (Life Technologies).

MEKK1 and P38 inhibitor studies

For inhibitor studies, HSVSMC were plated and quiesced for 48 h. One hour prior to stimulation, cells were incubated with either 10, 15 or 20 μM AZD6244 (MEKK1 inhibitor, Selleckchem, Suffolk, UK) or 5, 10 or 20 μM P38 (SB 203580). Cells were then maintained in either 0.2% media or stimulated with a combination of IL1α and PDGF for 24 h before RNA isolation.

5' and 3' RACE

5' 3' Rapid amplification of cDNA ends [1] was performed to determine the full length transcript of SMILR using the SMARTer RACE 5'/3' Kit (Clontech, Saint-Germain-en-Laye, France) according to manufacturer's instructions. Nested PCR was used to ensure only specific 5' and 3' products were detected (*PCR Primer sequence – Suppl. Table 1*). Following cloning into supplied cloning vector, products were sequenced.

Fluorescent *in situ* hybridisation

Custom RNA-FISH tiled probe sets were generated to all exons of SMILR. RNA FISH utilises "branch tree" technology. Briefly, a target specific probe set, containing 40 oligo probes, hybridises to the target mRNA as 20 oligo pairs. Each oligo pair forms a required platform for assembly of the signal amplification structure (tree) through a series of sequential hybridisation steps. Each fully assembled structure, covers a space of 40-50 nt of the target RNA, and has the capacity for 400-fold signal amplification. Therefore, a typical RNA probe set (containing 20 oligo pairs) has the capacity to generate 8,000-fold signal amplification. Due to this technology the company confirms single-molecule RNA sensitivity, thus each fluorescent signal corresponds to an individual lncRNA molecule.

Control SNORD3 and UBC were used as housekeepers to determine spatial location of SMILR (Panomics, Affymetrix, California, US). RNA-FISH was performed according to manufacturer's instructions (ViewRNA^{TM} cell FISH) with minor modifications for both cell and tissue experiments. For cellular analysis, HSVSMC ± IL1α/PDGF were grown on 16-mm coverslips to 80% confluency, washed in PBS and fixed in 4% paraformaldehyde supplemented with 1% glacial acetic acid. Following detergent QS permeabilisation and 1:6000 protease digest, coverslips were incubated with a combination of UBC and SMILR probe sets or UBC. Probe set buffer was used as a negative control and SNORD3 as confirmation of nuclear permeabilisation. Following probe hybridisation, cover slips were incubated with branched tree technology pre amplifier for 1 h and amplifier for 30 min. Cover slips were finally incubated with fluorescent probes, mounted onto glass slides using Prolong gold anti-fade with DAPI mounting medium (Life Technologies).

Image acquisition

Images acquired on a Zeiss 510 confocal system. At least 5 images were taken per condition. Parameters for acquisition and post analysis were identical for all conditions. Images were Z stacked to confirm nuclear localisation.

Dicer substrate siRNA (dsiRNA) mediated transfection

Double stranded dicer substrate siRNA targeting SMILR and Si-control were synthesised (Integrated DNA Technologies, Leuven, Belgium). The Si-control does not target any sequence in the human, mouse, or rat transcriptomes. Transient transfection was performed with Lipofectamine 2000 (Life Technologies). Cells were transfected with either 25 nM Si-SMILR or Si-Control. Six hours post transfection, cells were quiesced for 48 h and stimulated for a further 48 h with 0.2% media containing IL1α/PDGF.

Lentiviral mediated infection

Lentiviral vectors were produced by triple transient transfection of HEK293T cells with a packaging plasmid (pCMVΔ8.74), a plasmid encoding the envelope of vesicular stomatitis virus (VSVg) (pMDG) (Plasmid Factory, Bielefeld, Germany) and pLNT/SFFV-MCS plasmid employing polyethylenimine (PEI; Sigma-Aldrich, St Louis, USA) as previously described. Lentiviral titres were ascertained by TaqMan quantitative real-time PCR (qRT-PCR) using the following primer/probe sequences: forward, 5'-TGTGTGCCCGTCTGTTGTGT-3'; reverse, 5'- GAGTCCTGCGTCGAGAGAGC-3'; probe, 5'-(FAM)-CAGTGGCGCCCGAACAGGGA- (TAMRA)-3. SMILR was cloned into the pLNT/SFFV-MCS (kind gift from Adrian J. Thrasher, London, UK) plasmid using Platinum taq polymerase, according to manufacturer's instructions, to create pLNT/SFFV-MCS-SMILR. A confluent monolayer of smooth muscle cells were plated and infected with a multiplicity of infection of either 25 or 50, neither of which induced any form of toxicity in our cells. Following 24 h infection, media was changed to 0.2% for a further 48 h. Cells were then stimulated and EdU incorporation or SMILR expression investigated as above.

Detection of LncRNA in exosomes secreted from HSVSMC

SMILR expression in conditioned media utilising both ultracentrifugation and exosome isolation kits. RNA extraction of exosome free HSVSMC media was performed using a standard volume (15 mL). The conditioned media was centrifuged at 2000 g at 4°C for 10 min and then at 12000 g for 45 min to remove all cell debris. The supernatant was filtered (0.22 μm) followed by ultracentrifugation at 110 000 g, 4°C for 90 min (Optima L-80 XP ultracentrifuge Beckman coulter) to obtain microvesicles (MV) and exosomes and exosome free media compartments. Additional experiments were performed utilising the Total exosome isolation kit (Life technologies) following the manufacturer's instructions. The presence of microvesicles and exosomes was verified using the Nanosight technology

For exosomes and microvesicles, 700 µL of Qiazol (Qiagen) was added and 3 µL of c.elegans total RNA at 25 ng/µL and the RNA was extracted using miRNEasy mini kit (Qiagen) as previously described. For the exosome free media compartment, RNA was extracted from 2 mL and following the same protocol as describe in the manuscript. SMILR relative expression was determined in theses 2 compartments by qRT-PCR.

In Vivo Studies Atherosclerosis Studies: Patients, Imaging and Sampling

Carotid cohort

Patients with symptomatic carotid artery stenosis (≥50% by NASCET criteria [2]) scheduled to undergo carotid endarterectomy were recruited from neurovascular clinics at the Royal Infirmary of Edinburgh between January 2013 and April 2014. Exclusion criteria included a modified Rankin score of 3, insulin-dependent diabetes mellitus, women of child-bearing age not receiving contraception, severe chronic kidney disease (eGFR <30 mL/min/1.73 m^2), known iodine-based contrast media allergy, prior ipsilateral carotid intervention, prior neck irradiation, and inability to provide informed consent. Patients underwent a standard baseline clinical assessment including blood sampling (for standard clinical haematological and biochemical indices, including C reactive protein, and plasma RNA analysis) before undergoing separate [18F]-fluoride and [18F]-fluorodeoxyglucose ([18F]-FDG) positron emission tomography [3] combined with computed tomography (CT) scans with the use of a hybrid scanner (Biograph mCT, Siemens Medical Systems, Erlangen, Germany). Both of these tracers have been used by our group and others for plaque imaging and highlight high-risk actively calcifying [4] and inflamed or hypoxic atherosclerotic plaques.

For [18F]-fluoride imaging, a target dose of 250 MBq was administered intravenously. Scanning took place after a 60-min delay. Following an attenuation-correction CT scan (non-enhanced, low dose 120 kV, 50 mAs) PET imaging was performed in static mode covering 2 bed positions (15 min each) with the superior bed centered over the carotid bifurcation.

Following PET acquisition, a CT carotid angiogram was performed without moving the patient (Care Dose 4D, 120 kV, 145 mA, rotation time 0.5 s, pitch 0.8).

[18F]-FDG PET/CT was performed on a separate day. A target dose of 125 MBq was administered intravenously and scanning commenced after a 90-min delay. PET/CT acquisition was identical to [18F]-Fluoride save for a longer bed time of 20-min and a pre-scan fast of 6 h. Static images were reconstructed using the Siemens Ultra-HD algorithm (time of flight + True X) with corrections applied for attenuation, dead time, scatter, and random coincidences.

PET tracer uptake was quantified using an OsiriX workstation (OsiriX version 3.5.1 64-bit; OsiriX Imaging Software, Geneva, Switzerland). PET/CT image data were reviewed for evidence of tracer uptake, image quality and registration. The CT angiogram was examined to establish plaque presence, location and characteristics. Regions of interest [5] were then drawn on three adjacent 3-mm PET slices to incorporate the internal carotid artery plaque. Three ROI were then drawn around adjacent healthy portions of carotid artery and the lumen of the SVC to derive control values for “normal” arterial uptake and the blood pool respectively. Arterial standardized uptake values (SUV) were recorded and also indexed to blood pool activity thus giving a target-to-background-ratio (TBR).

At the time of surgery, plaques were collected immediately following excision and photographed. Two-millimeter diameter core biopsy specimens for RNA analysis were taken from regions of focally high uptake on PET and from normal tissue at the periphery of the endarterectomy specimen. These, along with the main specimen, were immediately frozen and placed in an -80°C fridge for subsequent batch analysis. Patient characteristic found in Suppl. Table. 5.

Assessment of lncRNA in human plasma

A standard volume of each plasma sample (300 µL) was used to extract RNA. Five volumes of QIAzol lysis reagent (Qiagen) was added per extraction and supplemented with spike-in RNA controls: 3.5 µL of miRNeasy Serum/Plasma Spike-In Control at 1.6 x 108 copies/µL (C. elegans miR-39 miRNA mimic; Qiagen) and 3 µL of c.elegans total RNA at 25 ng/µL. Following 5-min incubation at RT, chloroform was added at equal volumes to the starting sample. Following centrifugation (15 min; 8000 g; 4°C) the clear upper aqueous phase was used to isolate RNA as above.

Supplemental Figures

LncRNA Name	Chromosomal Location	Ensemble ID	Forward Primer sequence	Reverse Primer sequence
SMILER	chr8:123426571-123440790	RP11-94A24.1	ACCTTGGAGGTCTTGGGAGT	TTGCAGACACCTTCCAAACA
LncRNA 4	chr15:68591128-68593343	RP11-709B3.2	AAAAACTGCCACCTGTGACC	TTGGTGTAGGTCTGGGGAAG
LncRNA 6	chr8:121066919-121068440	RP11-760H22.2	CTGCATTGGAGAGACAGGAAT	AAAGCTGAAACCCTAAAGTCATTG
LncRNA 7	chr3:177534653-177617012	RP11-91K9.1	TGGCTAGGAGGGGGTCTATC	CACGGTGGCTCACACTTTTA
LncRNA 8	chr7:35756084-35774497	AC018647.3	CCAAGGTGATGAGCACAAAA	AAAGGTGGCAGAGTCCTTGA
SMILER RACE			GATTACGCCAAGCTTTGCAAACATTGGGATCAGCCGTGA	GATTACGCCAAGCTTTCTCACAGCCATGCTCTGGCCATT

Supplemental Table 1: Sybr green primer sequences. Exon spanning lncRNA primers were designed to each lncRNA to ensure no genomic DNA was assessed during qRT-PCR.

0.2% VS IL1α

Categories	Disease or Function Annotation	p-value
Cellular Movement	cellular movement	$1.3x10^{-36}$
Cell Death and Survival	necrosis	$1.6x10^{-33}$
Cellular Growth and Proliferation	proliferation of cells	$2.4x10^{-28}$
Organismal Development	angiogenesis	$2.3x10^{-26}$
Cancer	growth of tumour	$6.7x10^{-25}$
Connective Tissue Disorder	arthropathy	$8.1x10^{-24}$
Inflammatory Disease	chronic inflammatory disorder	$1.4x10^{-22}$
Cellular Movement	leukocyte migration	$1.9x10^{-23}$
Inflammatory Response	Inflammatory response	$4.3x10^{-23}$
Gastrointestinal Response	Digestive system cancer	$6.9x10^{-23}$

Supplemental Table 2: IL1α stimulation Ingenuity Pathway analysis. Top 10 disease and functional pathways predicted to be altered by IPA in HSVSM cells stimulated with IL1α.

0.2% VS PDGF

Categories	Disease or Function Annotation	p-value
Cellular Growth and Proliferation	proliferation of cells	$2.5x10^{-29}$
Cell Death and Survival	apoptosis	$3.3x10^{-25}$
Cellular Movement	migration of cells	$5.3x10^{-23}$
Cardiovascular System Development	development of the cardiovascular system	$2.3x10^{-26}$
Organismal Development	angiogenesis	$7.1x10^{-21}$
Cellular Development	proliferation of tumour cell lines	$8.5x10^{-21}$
Cancer	cancer	$1.5x10^{-20}$
Cell Cycle	mitosis	$1.7x10^{-17}$
Cell Morphology	morphology of cells	$5.3x10^{-16}$
Tissue Development	growth of connective tissue	$6.7x10^{-16}$

Supplemental Table 3: PDGF stimulation Ingenuity Pathway analysis. Top 10 disease and functional pathways predicted to be altered by IPA in HSVSM cells stimulated with PDGF.

0.2% VS IL1α + PDGF

Categories	Disease or Function Annotation	p-value
Cellular Growth and Proliferation	proliferation of cells	$1.0x10^{-45}$
Cell Death and Survival	apoptosis	$7.2x10^{-44}$
Cancer	cancer	$1.2x10^{-37}$
Cellular Movement	migration of cells	$2.3x10^{-34}$
Gastrointestinal Response	digestive system cancer	$7.0x10^{-30}$
Cellular Development	proliferation of tumour cell lines	$8.5x10^{-28}$
Reproductive System Disease	tumour	$4.8x10^{-27}$
Cell Cycle	Cell cycle progression	$6.2x10^{-26}$
Cardiovascular System development	morphology of cells	$2.2x10^{-24}$
Cardiovascular System development	angiogenesis	$4.8x10^{-24}$

Supplemental Table 4: IL1α + PDGF stimulation Ingenuity Pathway analysis. Top 10 disease and functional pathways predicted to be altered by IPA in HSVSM cells stimulated with IL1α and PDGF.

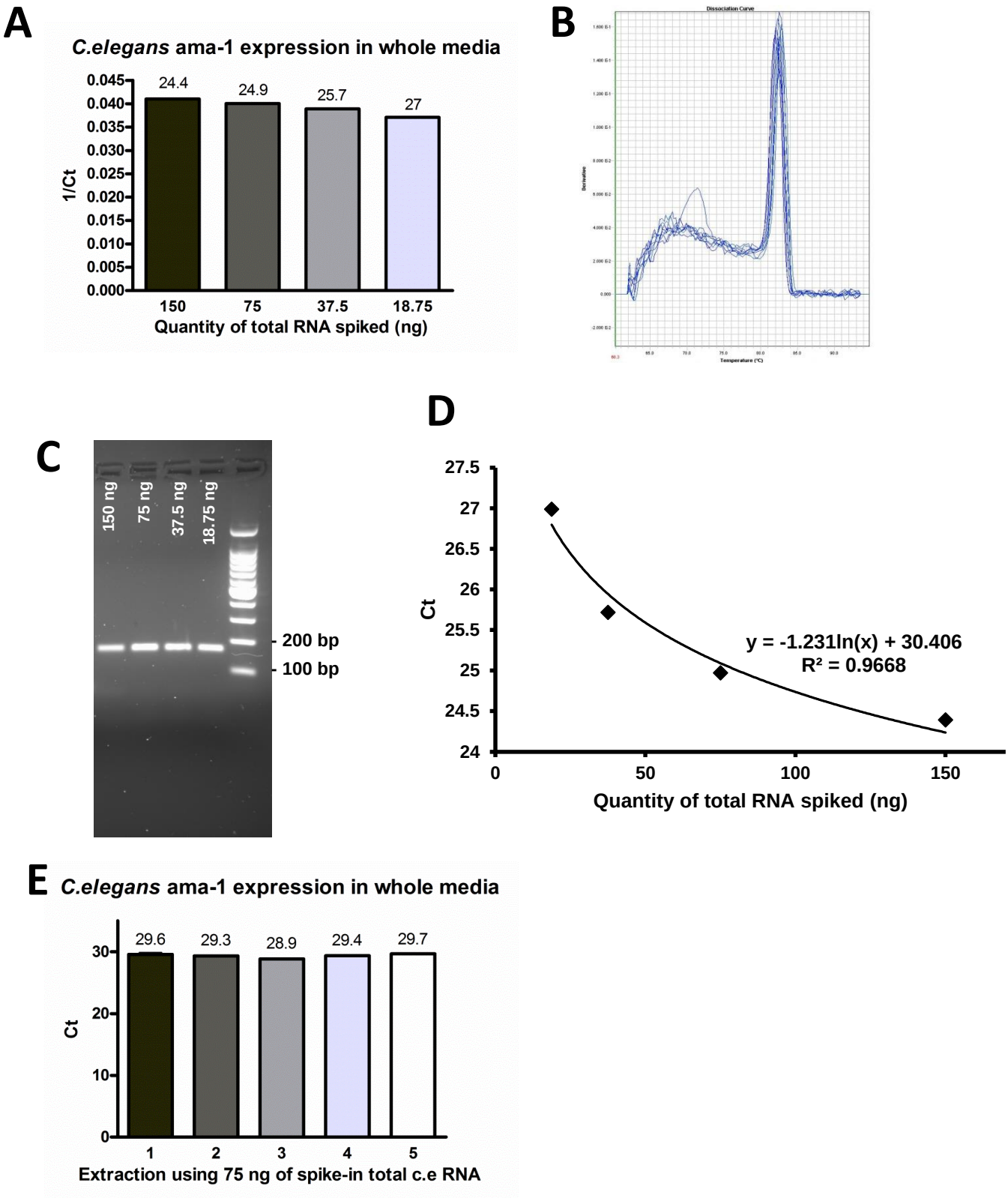

Supplemental Figure 1: Spike-in method of *C.elegans* total RNA in whole HSVSMC media. **(A):** Dose response effect of *C.elegans ama-1* expression. Expression determined by qRT-PCR and results displayed as 1/Ct. Number at the top of each histogram corresponds to Ct values. **(B):** Specificity of products analysis by melting curve. **(C):** Specificity of products analysed using agarose gel. The cDNA amplicon size has been resolved by migration on a 2% agarose gel using 100 bp ladder. **(D):** Correlation between quantity spike-in and *ama-1* expression. *C.elegans ama-1* expression follow a logarithmic function: y=-1.231ln(x)+30.406 with a coefficient of correlation r^2=0.9668. **(E):** Reproducibility of the technique. Following RNA extraction after 75 ng of spike-in total *C.elegans* RNA, *ama-1* expression was determined by qRT-PCR and the results have been displayed as Ct.

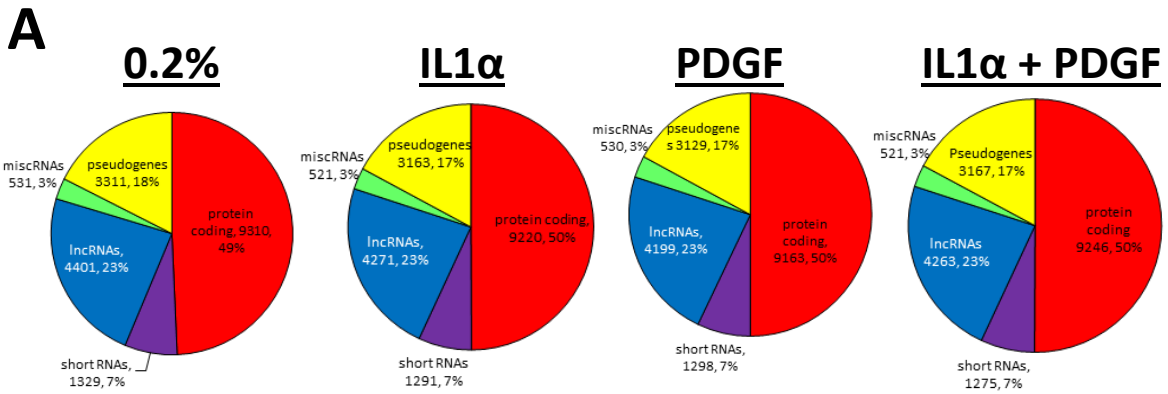

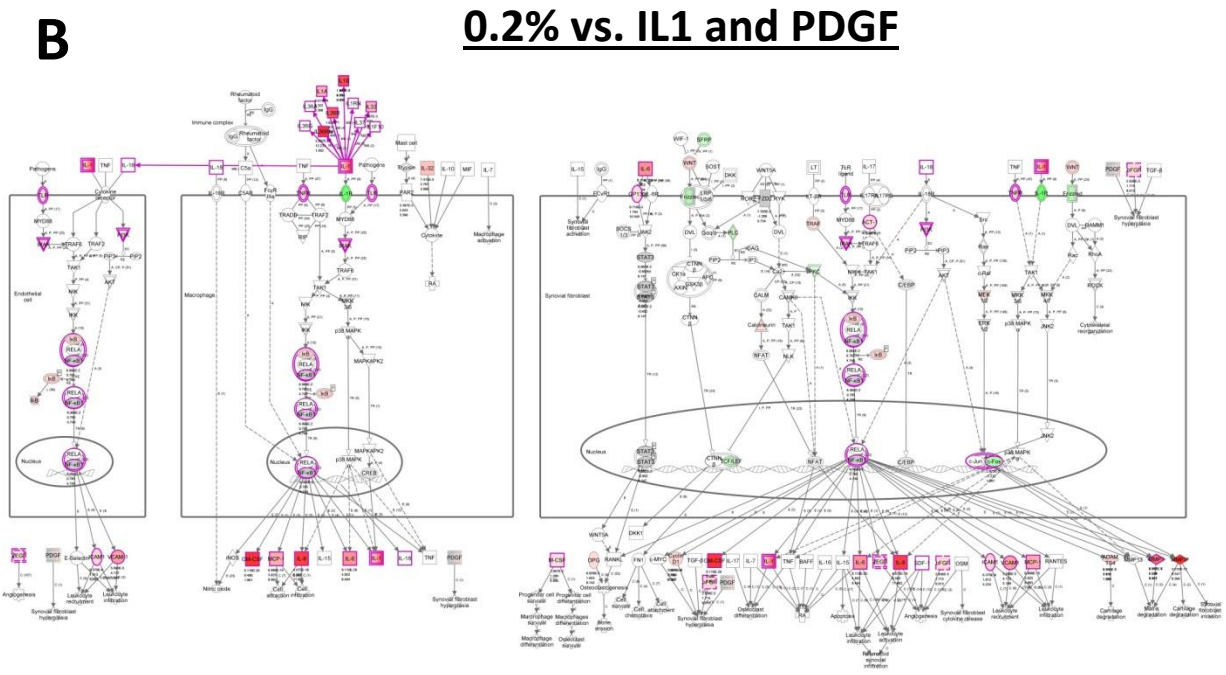

Supplemental Figure 2: **Assessment of RNA-seq data. (A):** Biotype distribution of all transcripts identified by RNA-seq analysis generated from HSVSM cells treated with IL1α and PDGF, cutoff at FPKM>0.1 **(B):** IPA analysis of top protein coding genes following IL1α and PDGF treatment.

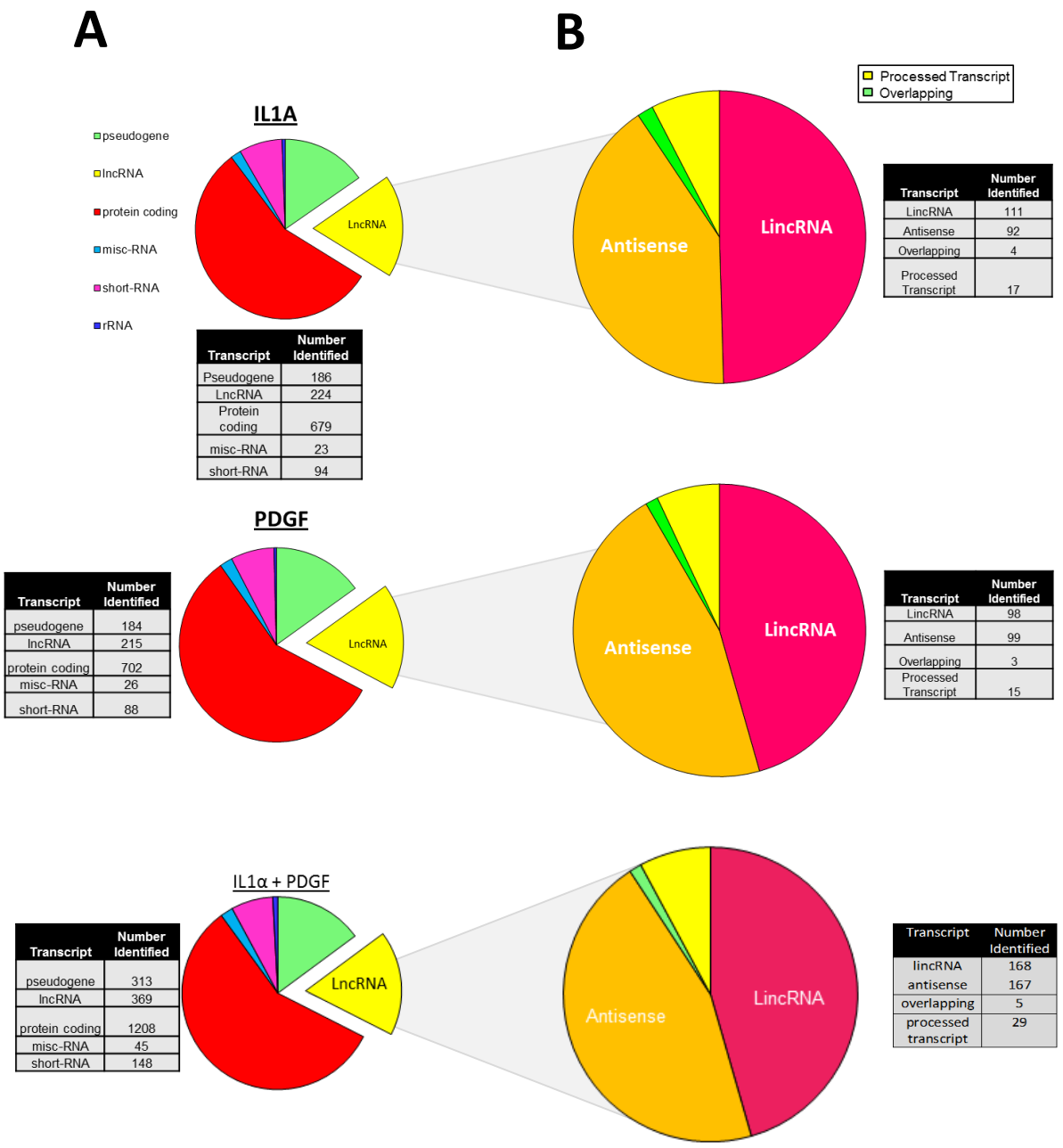

Supplemental Figure 3: **Identification of differentially expressed LncRNAs in HSVSMC treated with IL1α and PDGF.** Transcripts differentially expressed between 0.2% and stated treatment ($p<0.01$), pie chart indicates the relative percentage, and tables present numbers, of each biotype differentially expressed. LncRNAs differentially expressed between 0.2% vs IL1α/PDGF can be subdivided based on lncRNA biotype. Groups include intervening lncRNA (lincRNA), antisense, overlapping and processed transcripts.

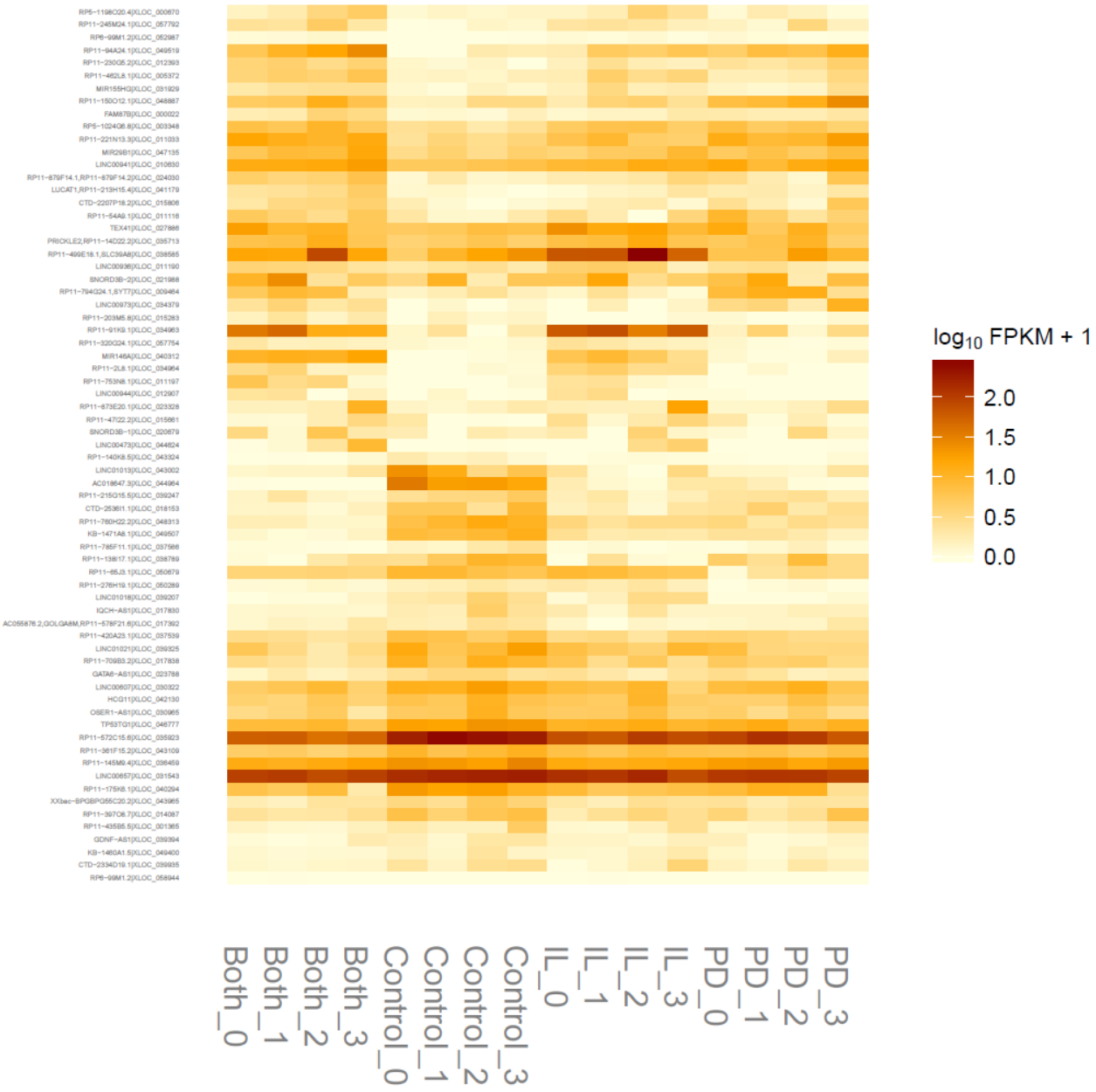

Supplemental Figure 4: **Heat map of most significantly dysregulated intervening lncRNAs across all treatment groups**. Heat map shows most significant changes in intervening lncRNA 0.2% vs IL1+PDGF treatment. LincRNA cut off using FDR<0.01, FPKM>1.

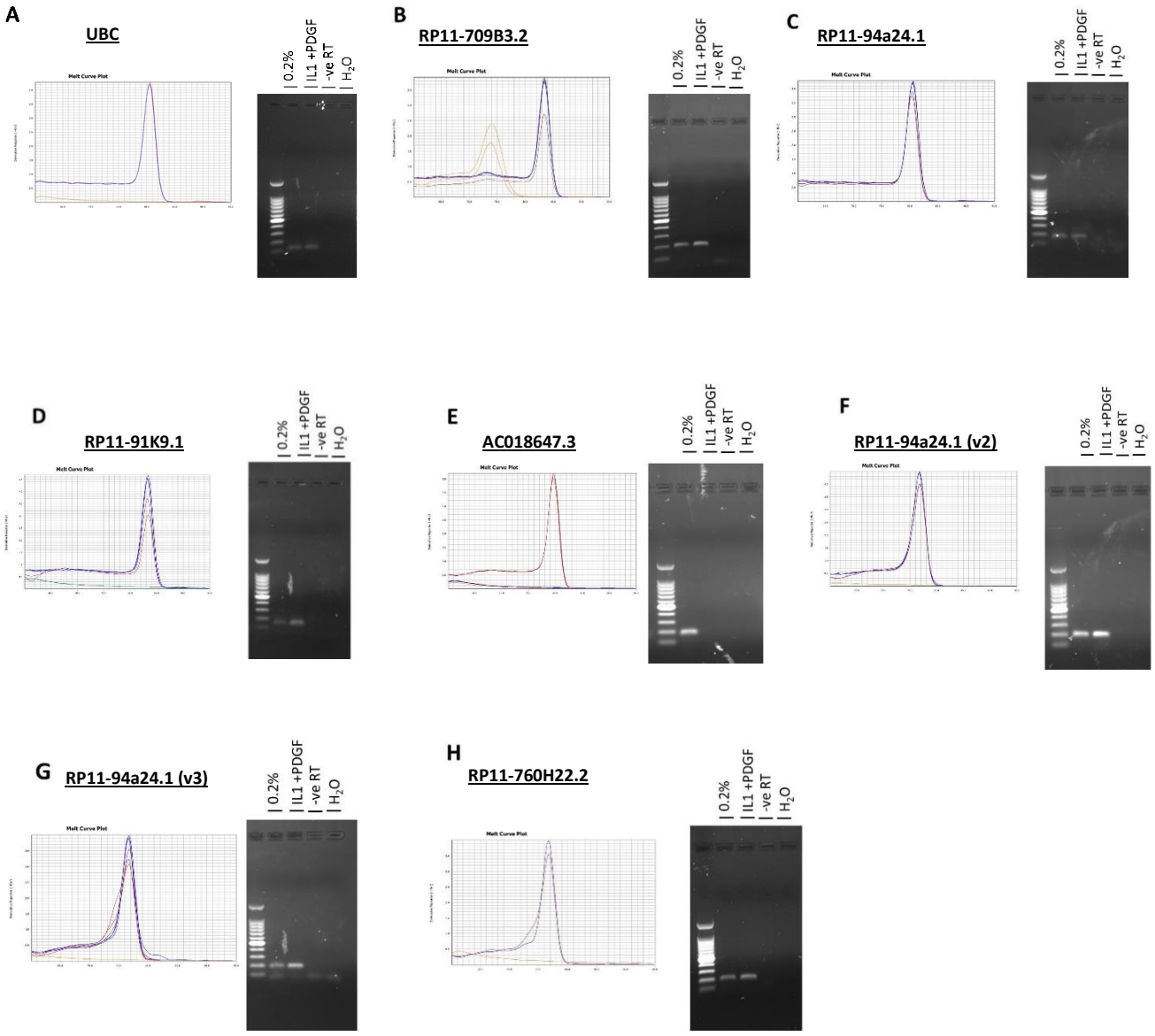

Supplementary Figure 5: Dissociation curves and gel products of PCR reactions indicating single PCR products. (A-H) Dissociation curves and gels for each lncRNA primer set. Primers were tested under 0.2% and IL1+PDGFconditions. Each gel also contains lanes containing –ve RT and H_2O samples.

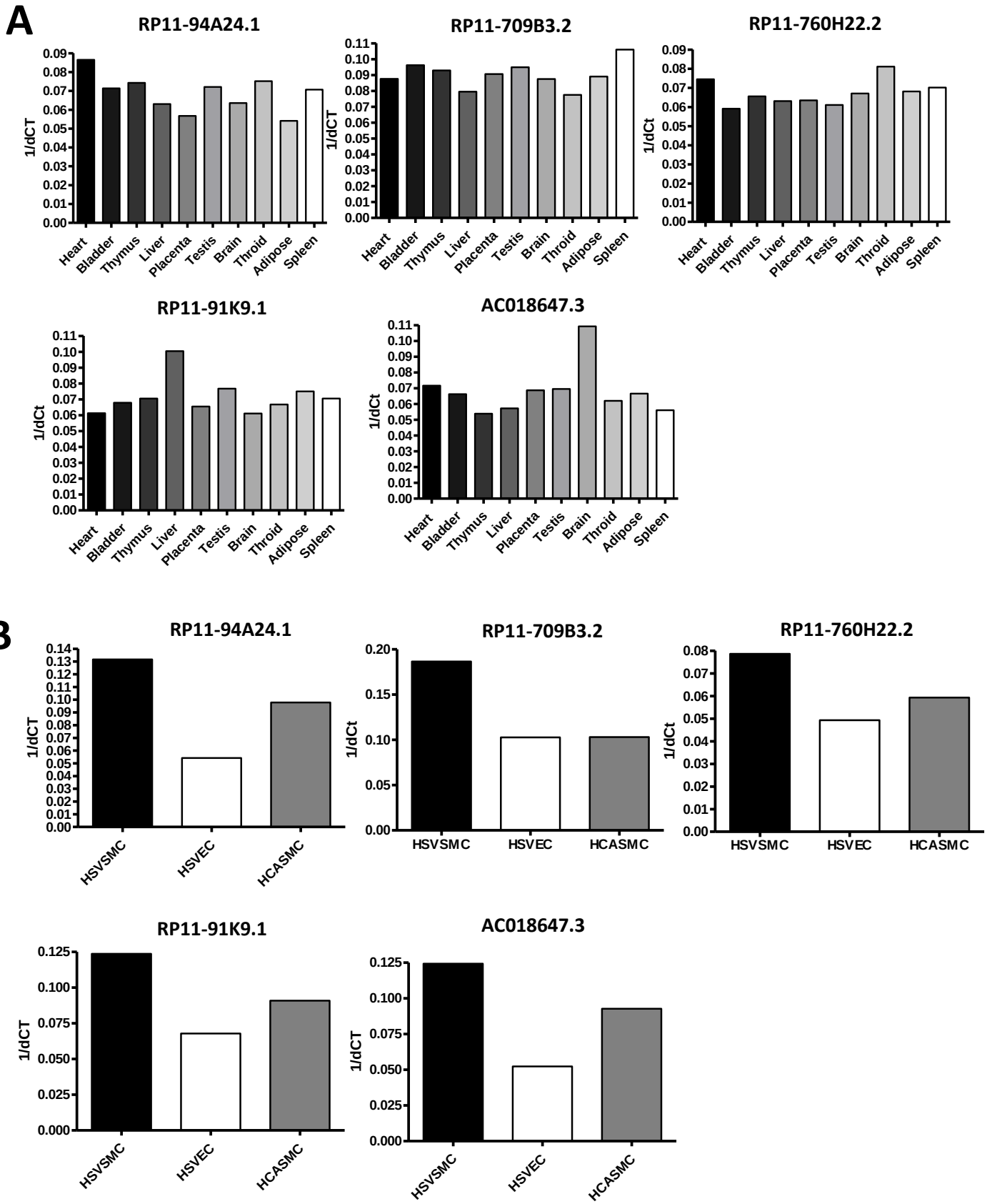

Supplemental Figure 6: LncRNA tissue and cell specificity analysis. (**A**): Expression of LncRNAs in a healthy tissue panel. Expression determined by qRT-PCR and results displayed as 1/ΔCT. (**B**): Expression of lncRNAs in unstimulated HSVSMC, HSVEC or HCAVSMC.

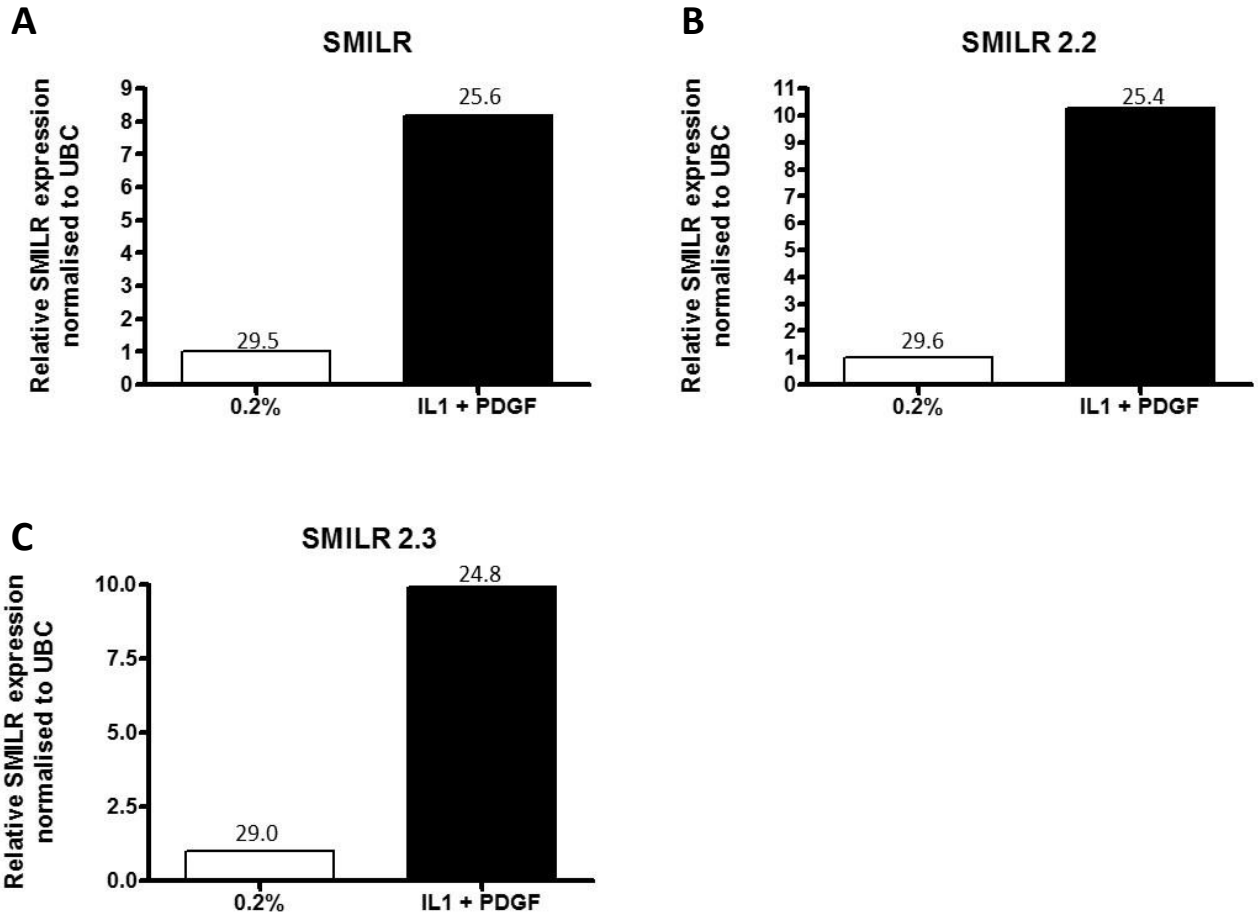

Supplemental Figure 7: Validation of additional SMILR primers. (A-C): Assessment of SMILR via qRT-PCR expression via 3 independent primer sets. The number on top of graphs represent Ct values obtained under 0.2% and dual stimulated conditions.

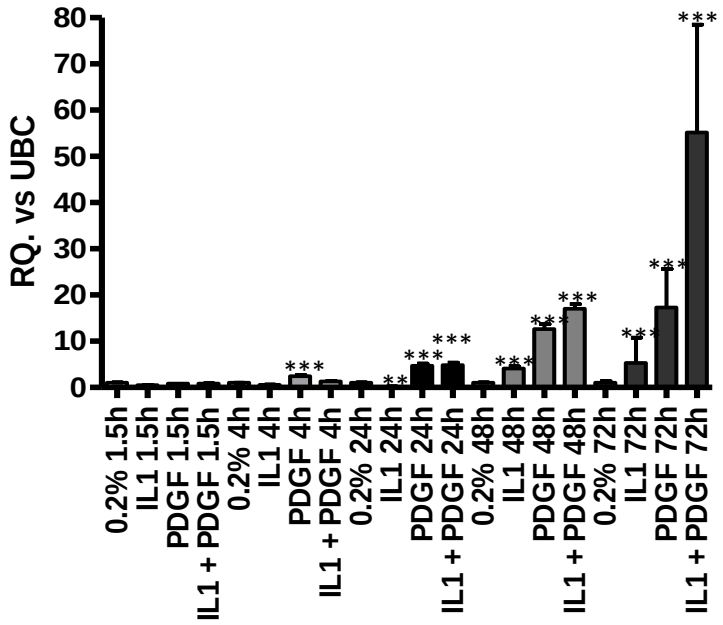

Supplemental Figure 8: **Temporal regulation of lncRNA 2 assessed by qRT-PCR.** HSVSMC were stimulated with IL1α, PDGF of a combination for the stated time points. RNA was extracted and expression determined by qRT-PCR.

A

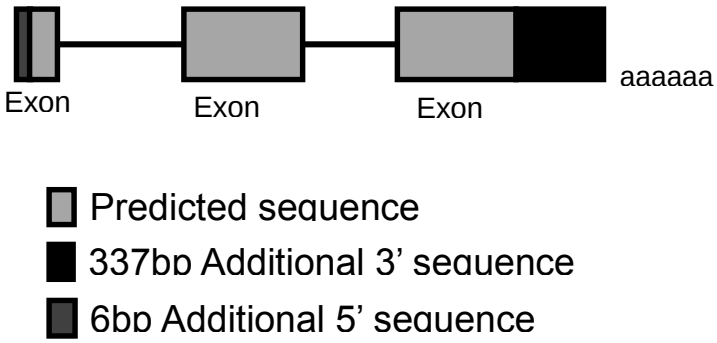

B

RP1194A24.1LncRNA2

GCTGCAAACATTGGGATCAGCCGTGACTATCCCATAACATAATATTTCTGATTTCATTCTTTT
CCTTTCTCCTACCAATTTAATCTGCAATCACTTCAAGAGAAGTCTGTTTAAAGGATATTCACA
TTCTG (intron1-11,398)
TTCACAGAGTTTGAGAGAAACTGTATTCAAGTTGCTGAAACCAAGAAGCTACACTCACGAGT
CTCACCTAAACTCGAATCTGATTTAGATGACATCATCCTGGACTTTGAGTTGATGAAACCTTG
GAGGTCTTGGGAGTAAAGCAAGTGTGATTTGCATATGATGGATATGAATTGTAATGGCCAGA
GCATGGCTGTG (intron 2- 2,269)
AGATGAAAACTCCCATTTTAGGGAACCAAGACTGAATTCCATAATTTACATGGATGTTTGGAA
GGTGTCTGCAACTTAATCTGTGTTCGTTTCTGAGATGTTGGGCAACTCCTTCTTGGAAGATG
TGGTAATGGTCTCTTCGAAAAGAAAATAATCATCTGAGTTTTGGCCAAAATAGTTGATCGGAT
TACCTATGAAAATGACTCTCACCCAACTACAAGAATGTTATGATGTAGAAACTCTAAATATAT
GAGTAATTAACTATACAACACTCCATCCCCATGTGAAAATCTTTAATCTTTTAAGATACTGAAA
TTTTGTGTATGTCTCATAATTTTCTGTATATGGTCAATGAGTTTTGCCTTAGCCATAAGTGGT
CTGTCTGAAATCTTCTCTATTATTTGTGCATTTTCTTCCTGATGTACCAAGCCTAGTCTGTTTG
TTTTTTCCTAAGAGAAAAGCAGATGATTCAACTGTGTATTTCTCAGTGTTGATATTGTGGTTT
GAGGTATTTCATAATCTTGAGTAAAATCTTGTCATAAAAAAAAAAAAAAAAAAAA

Supplemental Figure 9: **Visual representation of full *SMILR* transcript. (A):**Grey boxes indicate the predicted *SMILR* sequence obtained from UCSC genome browser (RP11-94A24.1) . Black boxes represent additional 316 basepair sequence obtained via 3' RACE of *SMILR* transcript. ***P<0.001, ** P<0.01 and * P<0.05 vs 0.2% in each time point (1 way ANOVA). **(B):** Full length sequence of lncRNA 2.

A

SMILR Raw RNA-seq Reads – Control (0.2%) and stimulated (IL1 + PDGF)

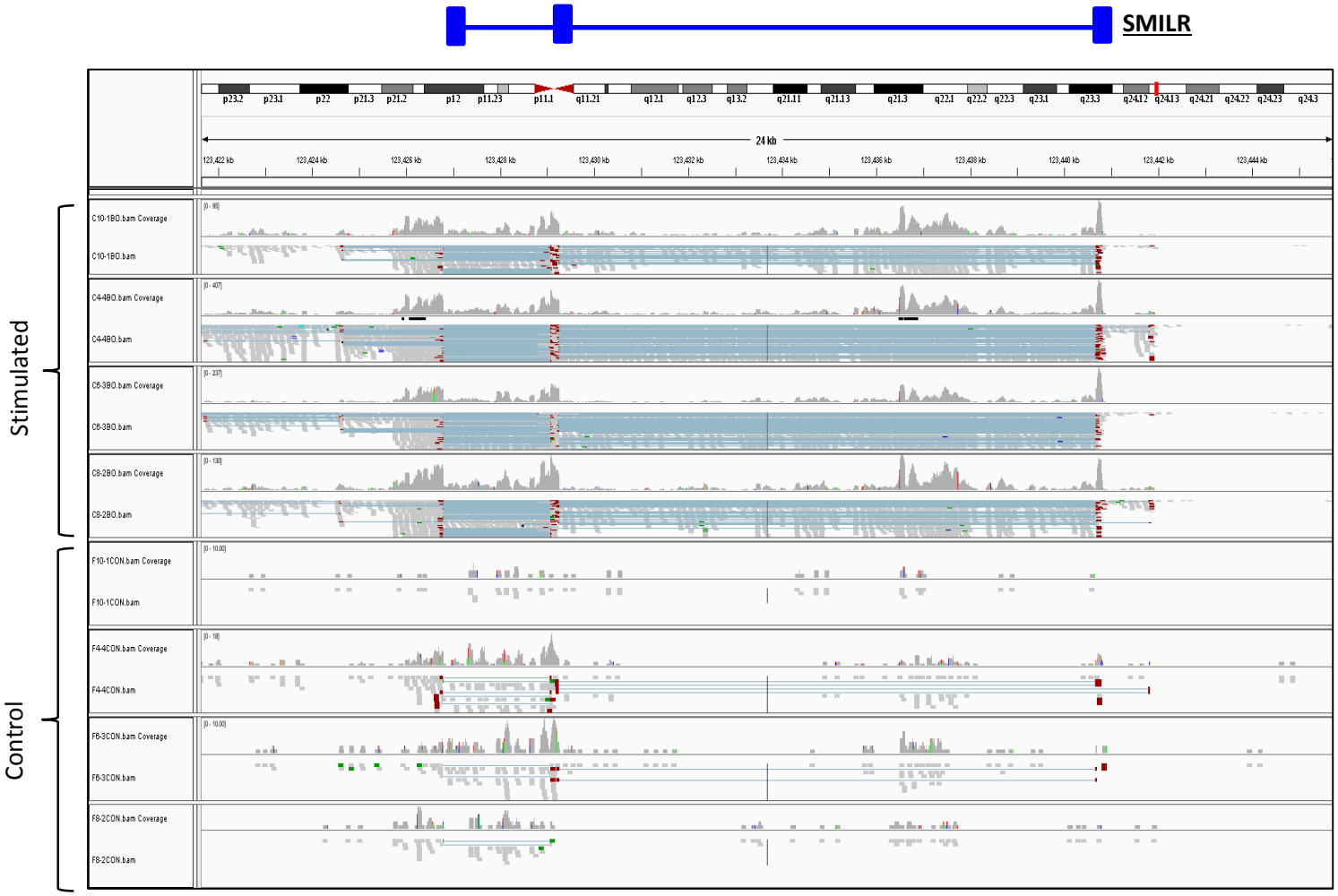

B ***HAS2 Raw RNA-seq Reads – Control (0.2%) and stimulated (IL1 + PDGF)***

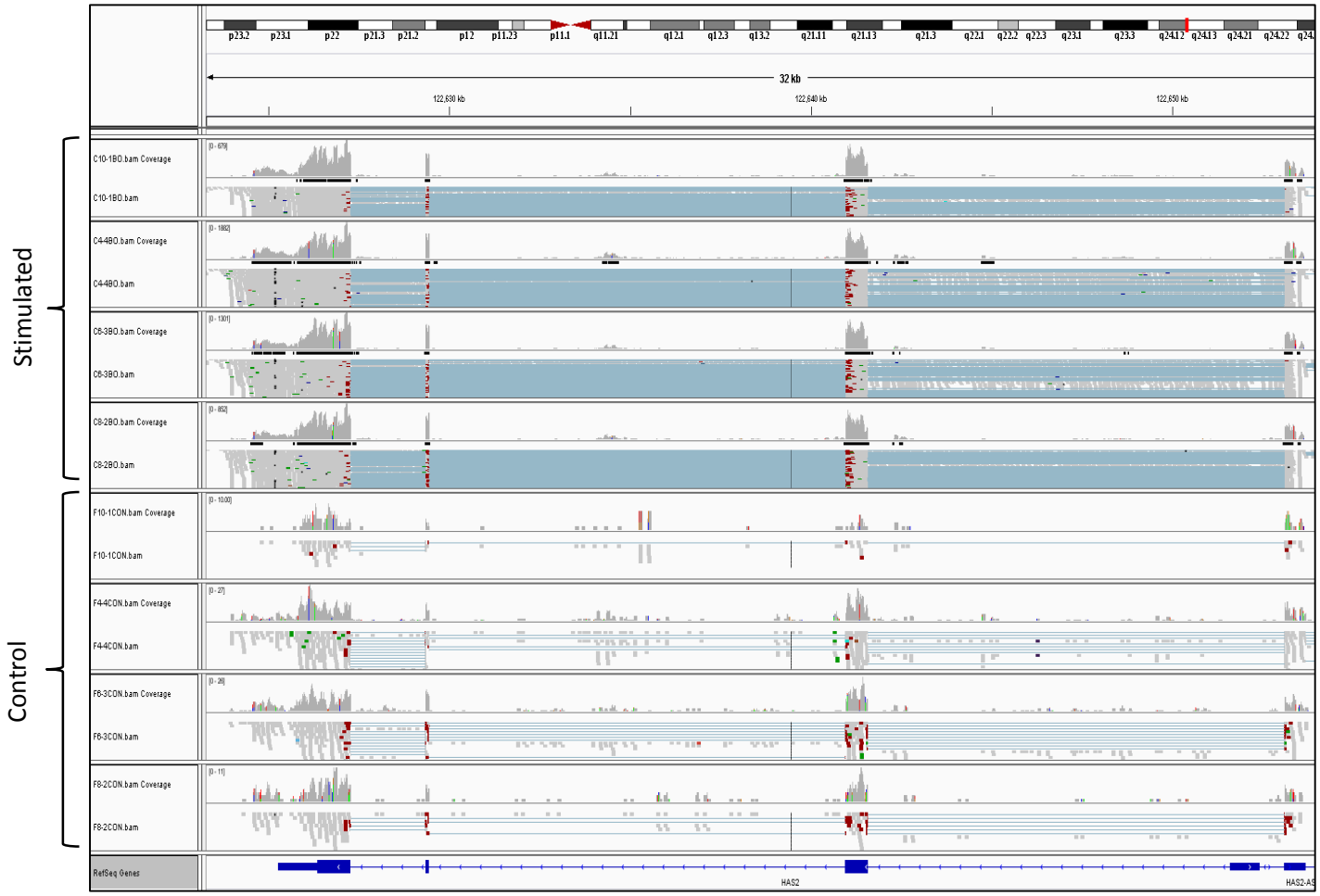

SMILR Raw RNA-seq Reads – Stimulated only – files expanded

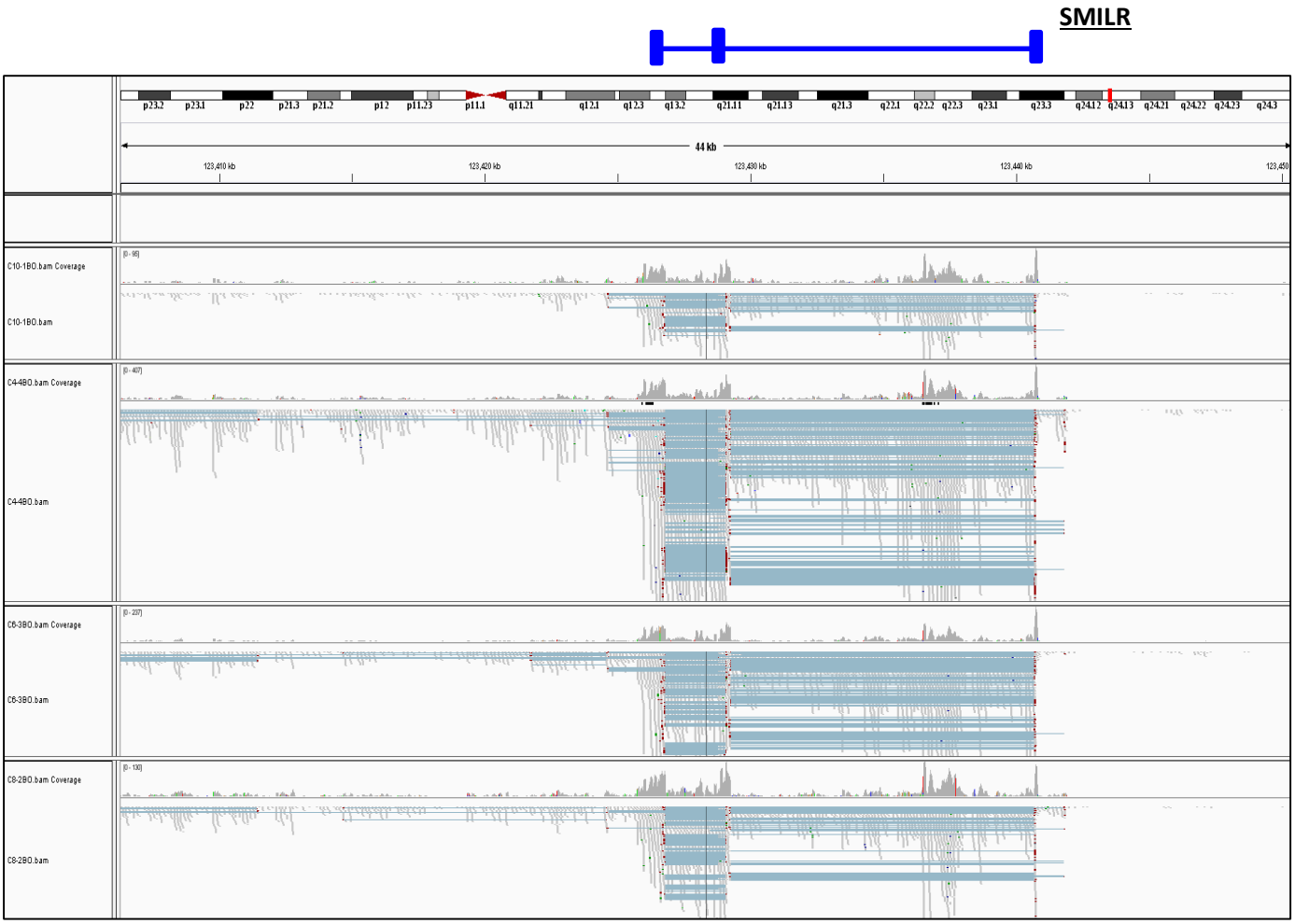

D

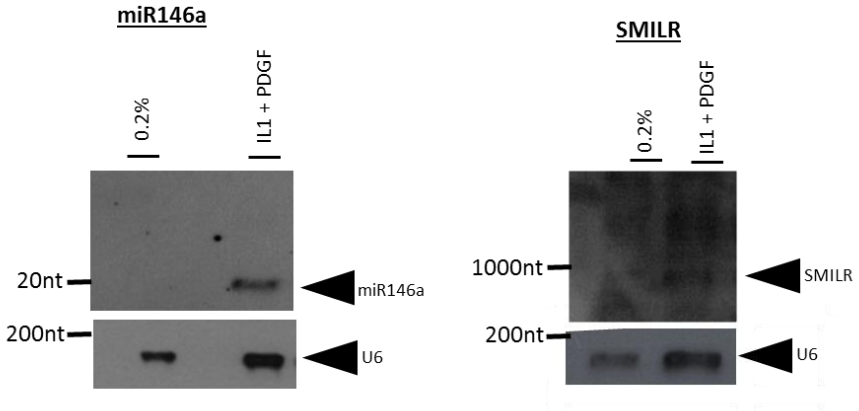

Supplemental Figure 10: Raw sequencing profiles generated utilising tophat files, constructed on integrative genome viewer (IGV). (A): Raw sequencing reads of SMILR under both basal and dual stimulated (IL1 + PDGF) conditions n=4. **(B):** Raw sequencing reads of HAS2 indicating a similar expression pattern following stimulation. **(C):** Raw sequencing reads of SMILR under stimulated conditions – expanded **(D):** Northern analysis of miR146a and SMILR RNA. U6 shown as loading control.

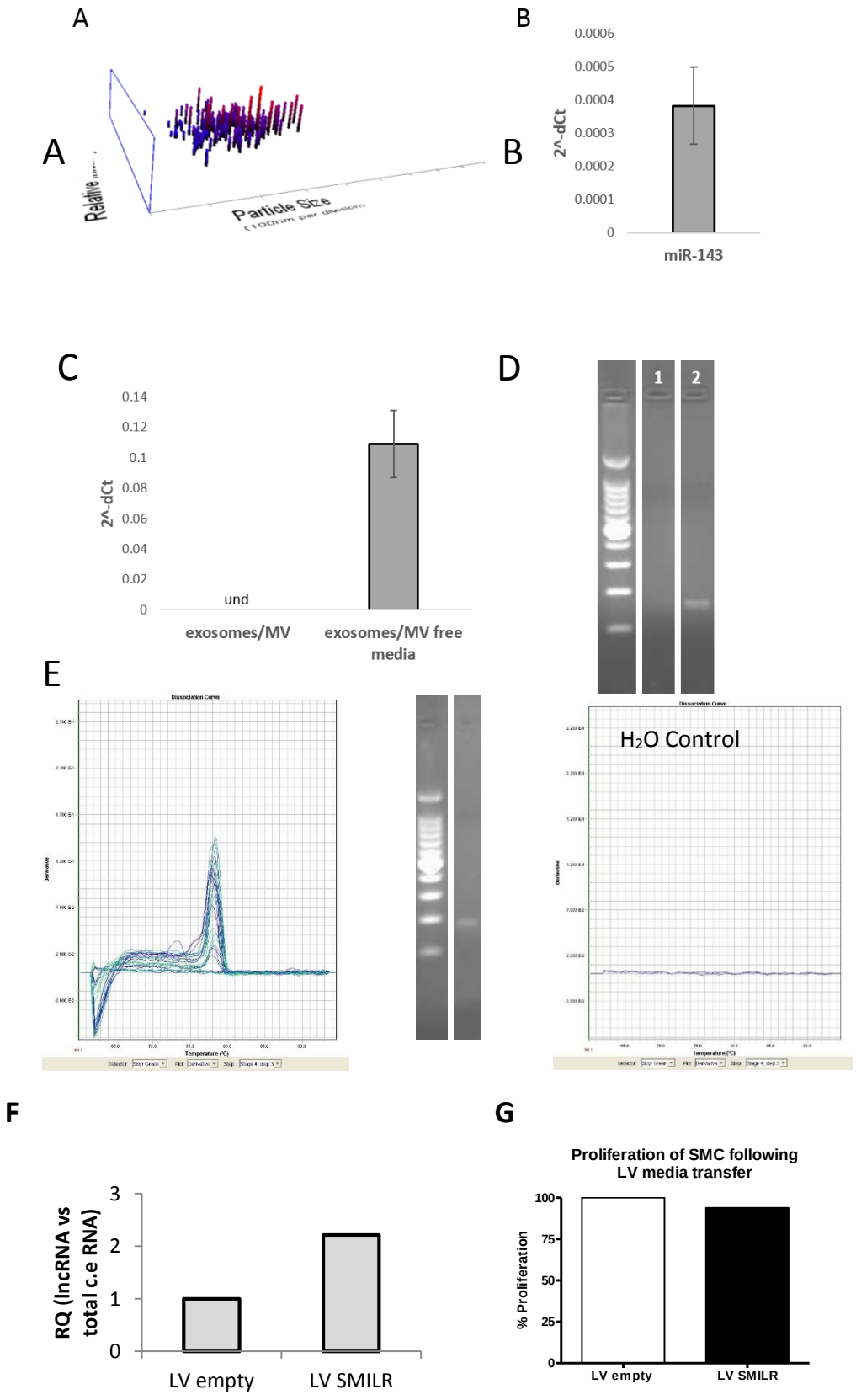

Supplemental Figure 11: Exosome isolation from HSVSMC conditioned media. (A): Size evaluation using the Nanosight of exosomes and MV isolated using the Total exosome isolation kit from 0.2% conditioned media. Sizes obtained between 70 and 600 nm. **(B):** Quantification of miR-143 in exosomes/MV isolated using the Total exosome isolation kit from 0.2% conditioned media. **(C):** SMILR expression analysed by qRT-PCR in exosomes/MV and exosomes/MV free media compartment from IL-1α + PDGF conditioned media. **(D):** Agarose gel of qRT-PCR products obtained in C; 1: exosomes/MV compartment, 2: exosomes/MV free media. **(E):** melting curves and gel electrophoresis of SMILR primer set in conditioned media**. (F):** SMILR expression from conditioned media following control lentivirus or SMILR lentivirus infection of cells. **(G):** Subsequent proliferation of quiesced cells following 48h incubation with lentivirus conditioned media.

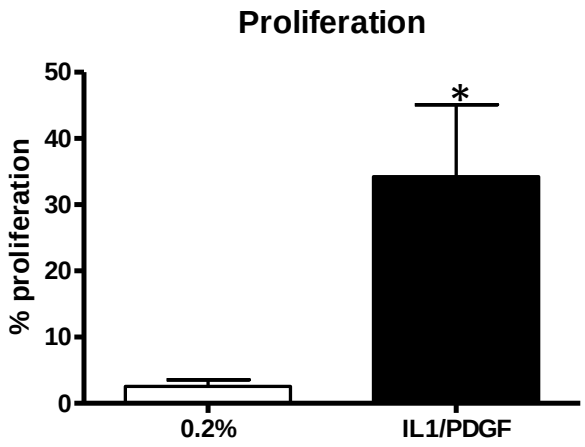

Supplemental Figure 12: Proliferation of HSVSMC 0.2% vs IL1 + PDGF treatment. P<0.05 students t test.

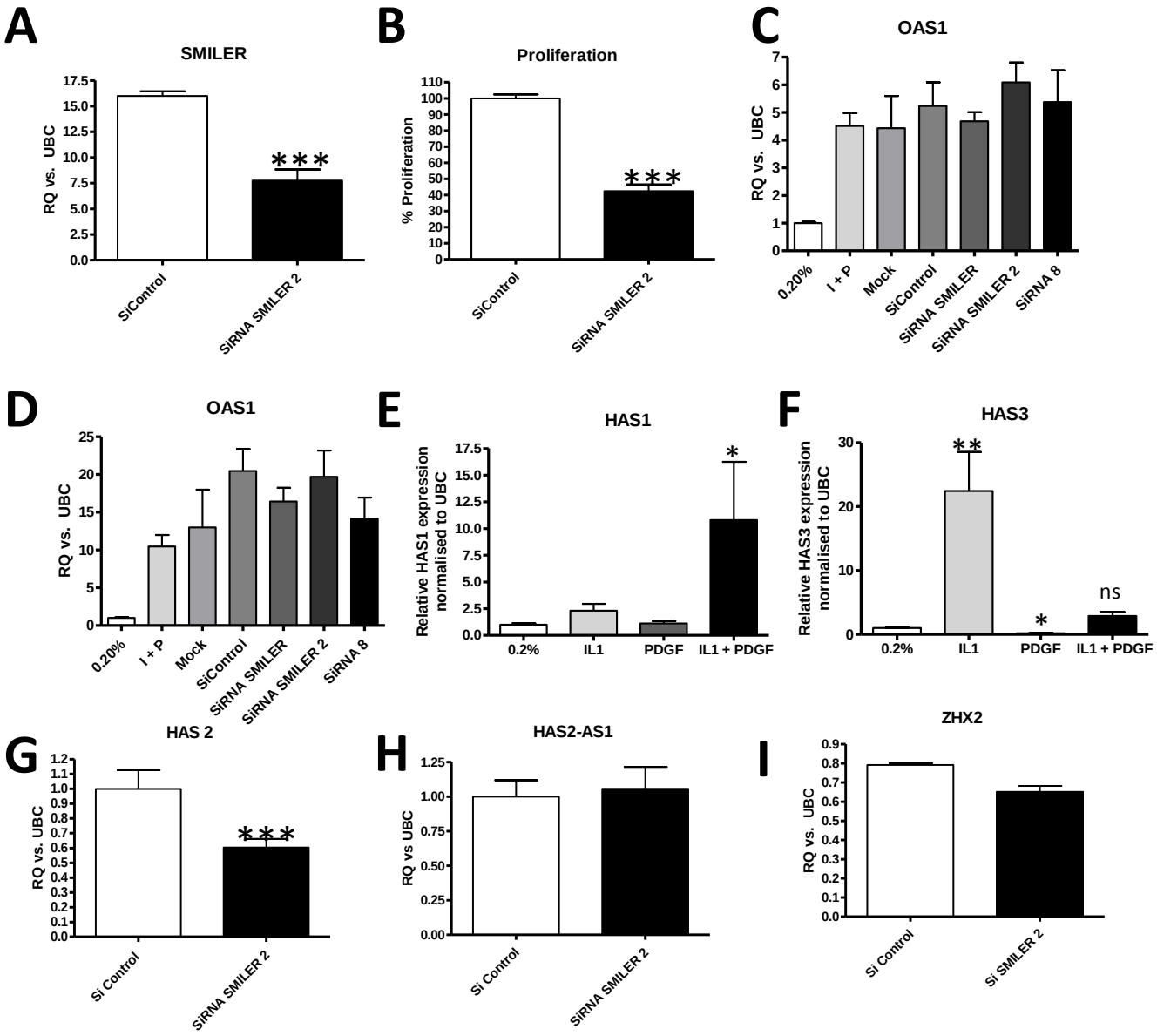

Supplemental Figure 13: (A): Confirmation of siRNA mediated down regulation of *SMILR* using second siRNA targeting a separate sequence of *SMILR*. **(B):** Confirmation of knockdown of *SMILR* using second siRNA. Analysed by students t-test ***P<0.001 vs SiControl. **(C-D):**qRT-PCR analysis of interferon gamma associated mRNA *OAS1* and *IRF7*. **(E-F):** qRT-PCR validation of *HAS1* and *HAS3* regulation by IL1α and PDGF. One way ANOVA *P<0.05. **(G-I):** Validation of siSMILR using second siRNA targeting different section of the lncRNA.

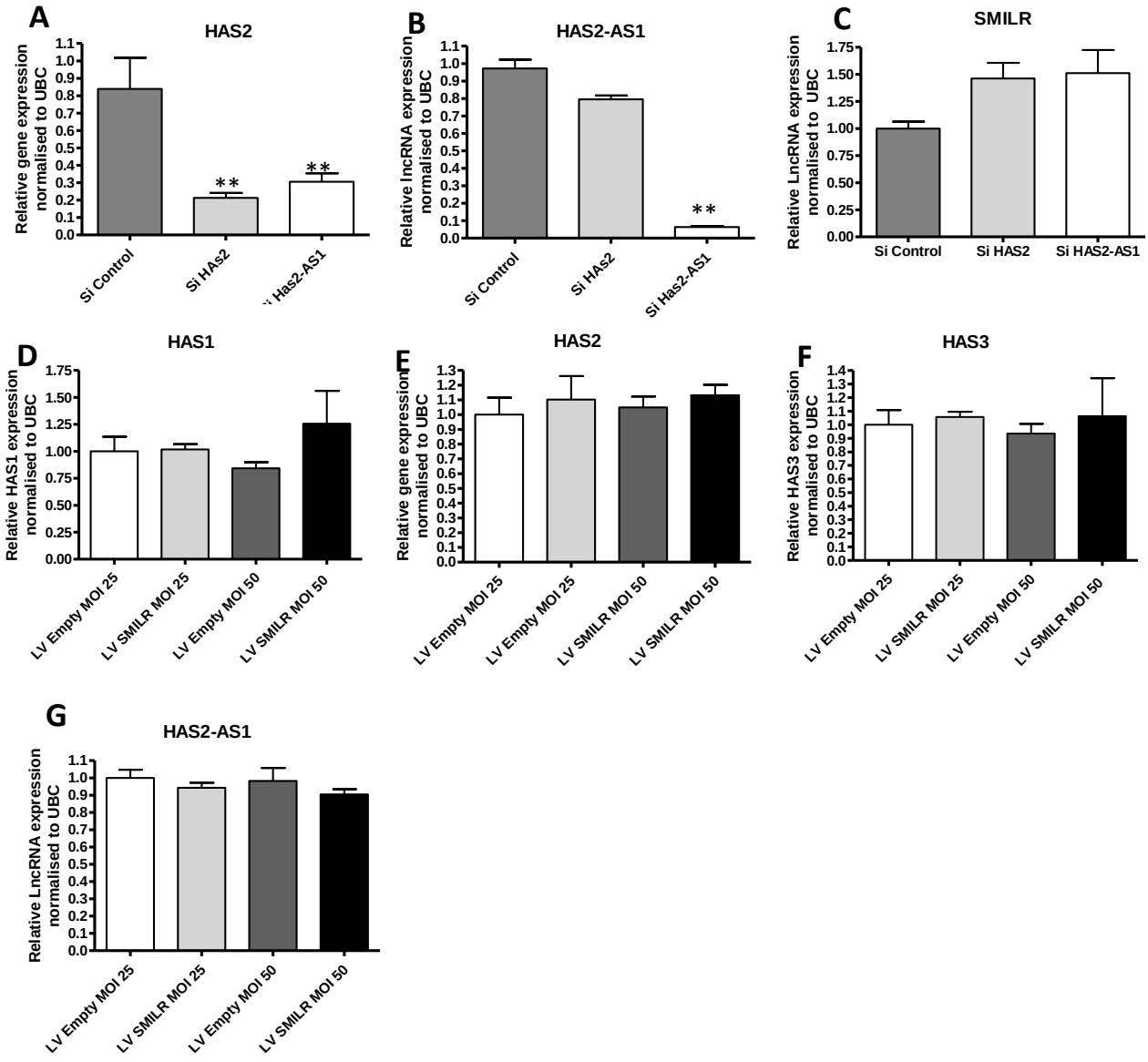

Supplemental Figure 14: Effect of HAS2 and HAS2-AS1 knockdown on SMILR expression. (A): Knocdown of HAS2 or HAS2-AS1 both reduced HAS2 expression. **(B):** Knockdown of neither HAS2 nor HAS2-AS1 affected SMILR expression levels. **(C):** Knockdown of HAS2 –AS but not HAS2 significantly reduced HAS2-AS1levels. **(D-F):** Overexpression of SMILR did not affect HAS1-HAS3 nor HAS1-AS1 expression levels.

	Carotid (n=7)
Age in years, mean (SD)	63 (13.8)
Men, n (%)	4 (57)
BMI (kg/m^2), mean (SD)	26.3 (5.8)
Systolic blood pressure (mmHg), mean (SD)	141.1 (22.5)
Diastolic blood pressure (mmHg), mean (SD)	88.4 (16.6)
Presenting syndrome, n (%)	
Stroke	2 (29)
TIA/Amaurosis fugax	5 (71)
Cardiovascular history, n (%)	
Ischemic heart disease	3 (43)
Myocardial infarction	1 (14)
Risk Factors, n (%)	
Hypertension	5 (71)
Diabetes	1 (14)
Hypercholesterolemia	7 (100)
Current smoker	3 (43)
Medication, n (%)	
Aspirin	2 (29)
Clopidogrel	5 (71)
Anti-coagulant	1 (14)
Statin	7 (100)
ACEi/ARB	3 (43)
B-blocker	2 (29)
Hematology, mean (SD)	
Hemoglobin	137.0 (23.1)
White cell count	8.1 (1.8)
Platelet count	284 (66)
Serum biochemistry, mean (SD)	
Creatinine (mmol/L)	90 (21.1)
Total cholesterol (mmol/L)	4.7 (1.3)

Supplemental Table 5- Baseline Patient Characteristics – Carotid Cohorts.

	group 1: crp<2 (n=13)	group 2: 2<crp<5 (n=13)	group 3: crp>5 (n=15)	*p* values
Age (years)	48.5 ± 1.8	48.5 ± 1.9	50.7 ± 2.1	0.66
CRP (mg/L)	1.24 ± 0.15	3.56 ± 0.28	7.09 ± 0.48	**p<0.0001**
Systolic BP (mmHg)	123 ± 2.9	131.2 ± 6.5	137.5 ± 4.6	0.12
Diastolic BP (mmHg)	77.5 ± 1.9	76.2 ± 2.0	79.0 ± 2.7	0.68
BMI (kg/m^2)	26.0 ± 0.5	28.7 ± 1.3	29.6 ± 1.7	0.14
WHR	0.96 ± 0.02	1.00 ± 0.02	0.99 ± 0.02	0.23
cIMT (mm)	0.64 ± 0.03	0.59 ± 0.03	0.64 ± 0.04	0.47
Smoking status, n (%)				0.015
Never smoker	61.5	61.5	60.0	
Ex-smoker	15.4	38.5	0.0	
Current	23.1	0.0	40.0	
SIMD quintile, n (%)				0.111
1	30.8	0.0	0.0	
2	23.1	7.7	6.7	
3	7.7	23.1	40	
4	7.7	15.4	13.3	
5	30.8	53.8	40	

Supplemental Table 6- Baseline Patient Characteristics – CRP matched plasma samples. Values are represented in mean ± SEM with *p* values calculated by one-way ANOVA or by Fisher's exact test for categorical variables.

SMILR in plasma

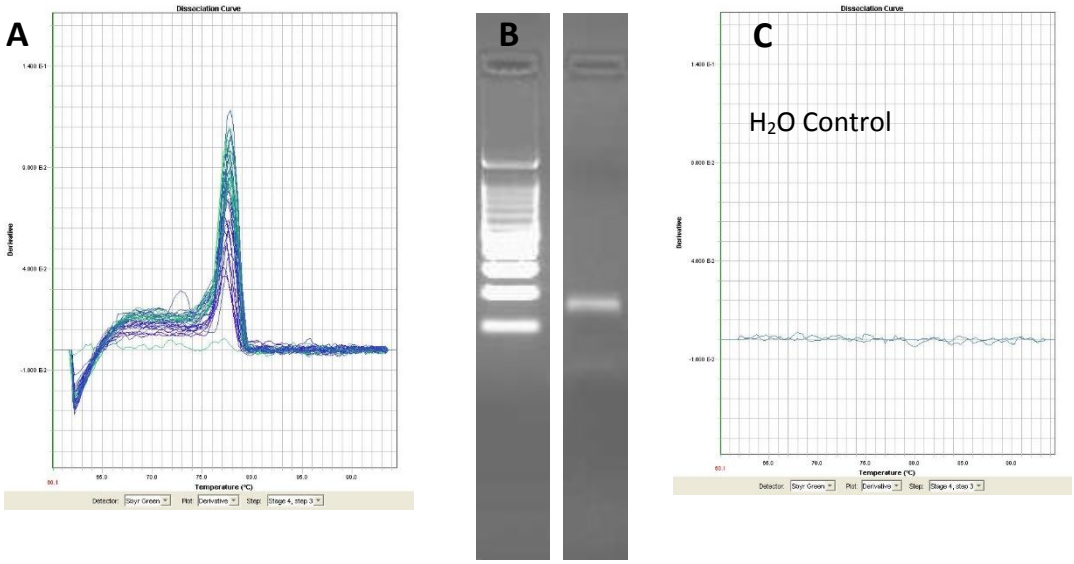

Supplemental Figure 15: Primer validation and quality control in plasma samples. (A): Melting curve for SMILR in plasma. **(B):** Agarose gel of qPCR product. **(C):** Water melting curve.

A The Pearson correlation:

		crp trans dct
Crp	1.0000	
Transdct	0.5719 0.0001	1.0000

So r=0.5719, r2=0.327, p<0.001

B If we take out the two outliers (the two highest dCts):

pwcorr crp transdct, sig

		crp trans dct
Crp	1.0000	
Transdct	0.389 0.0144	1.0000

r=0.389, r^2=0.151, p=0.014

Supplemental Figure 16: Statistical analysis of SMILR vs. CRP correlation. (A): Pearson correlation of SMILR vs. CRP utilising all data points. R=0.5719, r^2=0.327 and P<0.001. **(B):** Pearson correlation of SMILR vs. CRP omitting the 2 highest outlying points. R=0.389, r^2=0.151, p=0.014.

Supplemental References

1. Billings FTt, Balaguer JM, C Y, Wright P, Petracek MR, Byrne JG, Brown NJ, Pretorius M. Comparative effects of angiotensin receptor blockade and ace inhibition on the fibrinolytic and inflammatory responses to cardiopulmonary bypass. *Clinical pharmacology and therapeutics*. 2012;91:1065-1073
2. Hathout GM, Fink JR, El-Saden SM, Grant EG. Sonographic nascet index: A new doppler parameter for assessment of internal carotid artery stenosis. *AJNR. American journal of neuroradiology*. 2005;26:68-75
3. Upadhyay S, Ganguly K, Stoeger T, Semmler-Bhenke M, Takenaka S, Kreyling WG, Pitz M, Reitmeir P, Peters A, Eickelberg O, Wichmann HE, Schulz H. Cardiovascular and inflammatory effects of intratracheally instilled ambient dust from augsburg, germany, in spontaneously hypertensive rats (shrs). *Particle and fibre toxicology*. 2010;7:27
4. Irkle A, Vesey AT, Lewis DY, Skepper JN, Bird JL, Dweck MR, Joshi FR, Gallagher FA, Warburton EA, Bennett MR, Brindle KM, Newby DE, Rudd JH, Davenport AP. Identifying active vascular microcalcification by (18)f-sodium fluoride positron emission tomography. *Nature communications*. 2015;6:7495
5. Armand-Labit V, Meyer N, Casanova A, Bonnabau H, Platzer V, Tournier E, Sansas B, Verdun S, Thouvenot B, Hilselberger B, Doncescu A, Lamant L, Lacroix-Triki M, Favre G, Pradines A. Identification of a circulating microrna profile as a biomarker of metastatic cutaneous melanoma. *Acta dermato-venereologica*. 2016;96:29-34